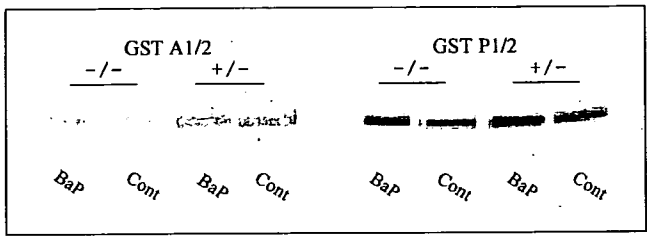

Figure 2. Immunodetection of GSTs. Cytosol fractions were extracted from the lungs of *nrf2*$^{+/-}$ (+/−) and *nrf2*$^{-/-}$ (−/−) mice, separated on SDS/PAGE, and electrophoretically blotted to Immobilon-P membrane. GST A1/2 and GST P1/2 were detected immunochemically using specific antibodies and ECL-plus system. BaP, cytosol fractions extracted from BaP-treated mouse lungs; *Cont*, cytosol fractions extracted from BaP-untreated mouse lungs.

the DNA repair system is quite efficient in the testis (22), metabolically active tissues, such as the liver and lung, seem to be unable to efficiently repair the DNA adducts produced by reactive oxygen species and/or endogenous mutagens without the presence of Nrf2. These results suggest that Nrf2 acts to suppress spontaneous mutagenesis in the lung and liver.

We aimed to quantitatively determine how Nrf2 deficiency affects mutagenicity *in vivo* in the lung using a single intratracheal instillation of BaP as a model environmental mutagen/carcinogen (13). BaP in cigarette smoke or ambient air is readily oxidized to reactive intermediates, such as BaP diol epoxide, by phase I detoxifying enzymes (23), and these intermediates are subsequently metabolized to hydrophilic conjugates by phase II detoxifying enzymes that are under Nrf2 regulation. However, unconjugated reactive intermediates, which often form, lead to DNA adduct formation (24). DNA adducts cause mispairing of DNA bases and induce gene mutations through the DNA replication process (25, 26). This process has been confirmed by *in vitro* experiment using BaP adduct-containing DNA as a template (27, 28). Indeed, a single intratracheal instillation of BaP into *gpt* delta mice resulted in a statistically significant and dose-dependent increase in the mutant frequency in the lungs of *gpt* delta mice, and the most frequent mutation induced by BaP was G:C to T:A transversion (13), which is characteristic of BaP mutagenesis (25, 26).

Therefore, *nrf2*$^{-/-}$*::gpt* and *nrf2*$^{+/-}$*::gpt* mice were given a carcinogenic dose (1 mg; ref. 29) of BaP through trachea, which resulted in a significant increase in the mutation frequency in lungs of both *nrf2*$^{+/-}$ and *nrf2*$^{-/-}$ mice. Importantly, BaP-treated *nrf2*$^{-/-}$ mice had a 2-fold higher mutant frequency ($2.93 \pm 0.56 \times 10^{-5}$) than BaP-treated *nrf2*$^{+/-}$ mice ($1.47 \pm 0.31 \times 10^{-5}$; Fig. 1*B*; Supplementary Table S2). The increment of mutant frequency by BaP treatment was higher in *nrf2*$^{-/-}$ mice than in *nrf2*$^{+/-}$ mice.

We thought that the expression level of Nrf2-regulated cytoprotective enzymes may explain both the higher basal mutant frequency in the Nrf2-deficient mouse and that following treatment of Nrf2-deficient mouse with BaP. Because Chanas et al. have shown that the class π GST isozymes are expressed at substantially lower levels in the livers of Nrf2-deficient mice than in wild-type mice (16). Because a thorough study of pulmonary GSTs in Nrf2-deficient mice has not been described in the literature, we decided to examine whether expression of GSTs was actually suppressed in the lungs of BaP-treated and BaP-untreated *nrf2*$^{-/-}$ mice by immunoblotting. In this study, we have examined expression of GST A1/2, GST A3, and GST P1/2, as these GSTs are known to be under the regulation of the Nrf2-ARE system (7) and are essential for the detoxification of BaP (30). Showing very good agreement with the report by Chanas et al. (16), which analyzed the expression of these enzymes in the mouse livers, the expression level of GST A1/2 was suppressed in the lungs of *nrf2*$^{-/-}$ mice compared with that in the *nrf2*$^{+/-}$ mice (Fig. 2), and the level of GST A3 was also low in Nrf2-deficient mice (data not shown). Under the experimental condition, GST A1/2 level was not elevated substantially by the BaP treatment in the lungs of *nrf2*$^{+/-}$ mice. Similarly, the expression level of GST P1/2 was also suppressed in the lungs of *nrf2*$^{-/-}$ mice compared with that in the *nrf2*$^{+/-}$ mice. GST P1/2 level was elevated by the BaP treatment in the lung of *nrf2*$^{+/-}$ mice, but there was no such difference in *nrf2*$^{-/-}$ mice. As the change in this immunoblotting experiment was relatively small, we repeated this experiment and found that the result was reproducible (data not shown). These results thus suggest that Nrf2 keeps the mutation frequency at low level in the lungs of mice by directing the expression the GSTs. As the changes in this GST immunoblotting experiments was relatively small, we speculate that lack of the

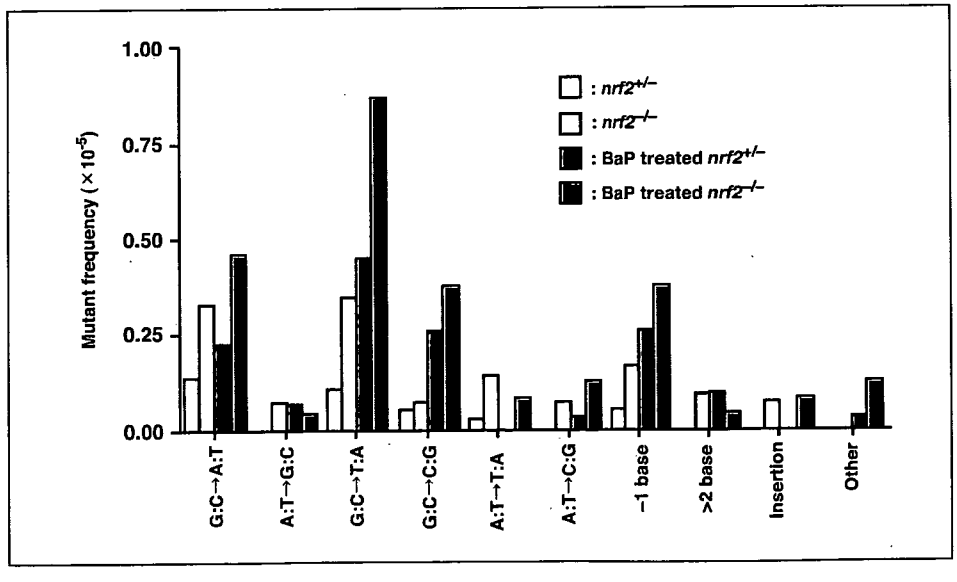

Figure 3. Comparison of mutant frequencies among the types of mutations in BaP-treated and BaP-untreated *nrf2*$^{+/-}$ and *nrf2*$^{-/-}$ mice. *Light blue column*, BaP-untreated *nrf2*$^{+/-}$ mice; *pink column*, BaP-untreated *nrf2*$^{-/-}$ mice; *blue column*, BaP-treated *nrf2*$^{+/-}$ mice; *red column*, BaP-treated *nrf2*$^{-/-}$ mice.

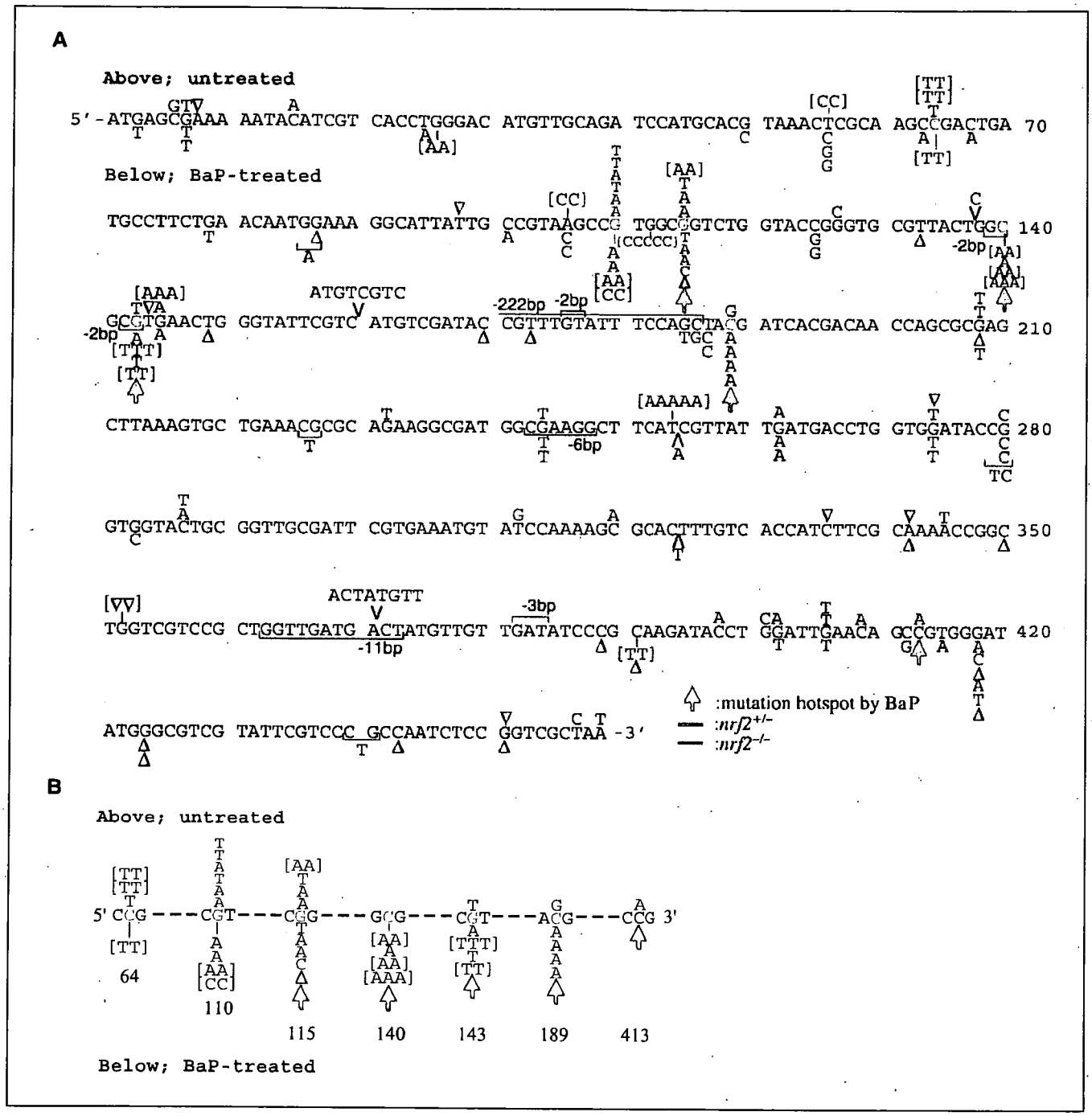

Figure 4. Overall distribution of the mutation detected on the *gpt* gene in the lungs of BaP-treated *nrf2*$^{+/-}$ and *nrf2*$^{-/-}$ mice and BaP-untreated *nrf2*$^{+/-}$ and *nrf2*$^{-/-}$ mice. The mutations are summarized in Supplementary Table S4. *A*, Mutations detected in *nrf2*$^{+/-}$ (*blue*) and *nrf2*$^{-/-}$ (*pink*) mice. The mutations detected in BaP-treated (*below* gpt *sequence*) and BaP-untreated mice (*above* gpt *sequence*). The number of characters in parenthesis is the number of mutations in one mouse. *Δ*, one base deletion; *half-boxes*, deleted nucleotides; *V*, a position of insertion. *Green arrows*, guanine nucleotides of BaP-induced mutation hotspots reported previously (13); *orange characters*, mutation hotspots found in this study. *B*, close-up of hotspots of mutations.

other Nrf2 target genes may also contribute to the mutant frequency in Nrf2-deficient mice.

To further characterize the mutational profile in the lungs of *nrf2*$^{-/-}$*::gpt* and *nrf2*$^{+/-}$*::gpt* mice after BaP exposure, we did DNA sequence analysis of 178 *gpt* mutant lung samples (Fig. 3; Supplementary Table S3). In *nrf2*$^{-/-}$ mice, the predominant spontaneous mutations were G:C to T:A transversion (26%, 15 of 58), G:C to A:T transition (24%, 14 of 58), and base deletions (19%, 11 of 58; Supplementary Table S3). A previous report of *gpt* delta mice (*mmh/ogg1::gpt*) suggested that accumulation of 8-hydroxyguanine in cells was the primary cause of increase in G:C to T:A transversion (31). 8-Hydroxyguanine may also play a role in the

induction of G:C to T:A transversion in the lungs of *nrf2*$^{-/-}$ mice because the level of antioxidant enzymes were suppressed in *nrf2*$^{-/-}$ mice, and subsequently, generation of reactive oxygen spices was probably accelerated.

The BaP treatment increased base substitutions at G:C pairs and one base deletion both in *nrf2*$^{+/-}$ and *nrf2*$^{-/-}$ mice (Fig. 3). Among the G:C substitutions, G:C to T:A and G:C to C:G transversions were markedly elevated in *nrf2*$^{-/-}$ mice after BaP treatment. Consistent with our previous studies with *gpt* delta mice (13), the predominant mutation provoked by BaP treatment was a G:C to T:A transversion (a major base substitute induced by the BaP-DNA adduct formation) in both *nrf2*$^{+/-}$ (32%, 14 of 44) and *nrf2*$^{-/-}$ (34%, 21 of 62) mice (Supplementary Table S2), and the mutant frequency of this transversion was higher in BaP-treated *nrf2*$^{-/-}$ mice than BaP-treated *nrf2*$^{+/-}$ mice (Fig. 3). In the lungs of *nrf2*$^{-/-}$ mice, DNA adducts are probably accumulated in the higher level than those in *nrf2*$^{+/-}$ mice because the expression levels of phase II enzymes that detoxify BaP by forming conjugates (32) and antioxidant enzymes are low in *nrf2*$^{-/-}$ mice comparing to *nrf2*$^{+/-}$ mice. We surmise that this increase of DNA adduct formation might elevate the mutant frequency of G:C to T:A transversion in the Nrf2-deficient condition. Additionally, generation of oxidative DNA adduct due to BaP-derived quinines (33) may be accelerated in *nrf2*$^{-/-}$ mice and play a role, albeit partly, in elevating the mutant frequency in *nrf2*$^{-/-}$ mice. Indeed, BaP adduct formation was accelerated ~2-fold in Nrf2-deficient mouse forestomach compared with wild-type mice (11), supporting our contention that the increase in the amount of DNA adduct enhanced the frequency of these transversions at G:C pairs.

To delineate the mode of mutation in Nrf2-deficient mice, the mutation positions in the *gpt* gene of BaP-treated and BaP-untreated mice were determined (Fig. 4*A*; Supplementary Table S4). Of the mutations found in BaP-treated mice (shown in lower side of the *gpt* sequence; Fig. 4*A*), G:C to T:A transversions at nucleotides 140, 143, and 189 were observed in three or more mice, including both *nrf2*$^{+/-}$ and *nrf2*$^{-/-}$ mice. Thus, these nucleotides are the hotspots of BaP-induced mutation. These nucleotides coincide with those previously reported (i.e., nucleotides 115, 140, 143, 189, and 413; ref. 13), which are shown with green arrows in Fig. 4*A*. The frequency of mutation at these hotspots was rather low in BaP-untreated mice (shown in upper side of the *gpt* sequence; Fig. 4*A*).

Because mutations were accumulated at relatively high level in the *gpt* gene of *nrf2*$^{-/-}$ mice even without BaP treatment, we assumed that we could assess hotspots of spontaneous mutation in these mice. Indeed, G:C to A:T transition at nucleotides 64 was observed in three BaP-untreated mice and one BaP-treated mouse. This mutation is exclusive in *nrf2*$^{-/-}$ mice. Thus, nucleotide 64 is the spontaneous mutation hotspot in Nrf2-deficient condition. In contrast, nucleotides 110 and 115 are common hotspots in BaP-treated and BaP-untreated mice; G:C to A:T transition at position 110 was observed in three BaP-untreated and three BaP-treated mice, and G:C to T:A transversion was also induced in three BaP-untreated mice.

Figure 4*B* shows mutation hotspots in the *gpt* gene. We found that one of the major trinucleotide sequences with BaP-induced guanine nucleotide mutation in this gene was CGT (nucleotides 110, 143, and 189). This is in good agreement with the previous observation that the instillation of BaP into the lung of *gpt* delta mice induced mutations frequently in CGT trinucleotide of the gene (13). CGG (nucleotides 64, 115, and 413) was another frequently found trinucleotide with guanine nucleotide mutations, but no link was found between this mutation and BaP treatment. It should be noted that guanine centered in CGC at position 140 was a frequent target of BaP-induced mutation in Nrf2-deficient condition, whereas previous experiments showed mutations were little in CGC of wild-type mice (13).

Whereas there was no significant difference in the mutation frequency, the position of the mutation was significantly different between BaP-untreated *nrf2*$^{-/-}$ mice and BaP-treated *nrf2*$^{+/-}$ mice (Fig. 4*A*; $P < 0.05$, Adams-Skopek test). This result suggests that chemical mutagenesis and spontaneous mutation in the *nrf2*$^{-/-}$ mice arise through different mechanisms. Thus, the Nrf2 deficiency had a marked affect on the mutational profile that arose either spontaneously or by BaP induction. However, further studies are required to clarify how Nrf2 deficiency alters the mutation profile, and whether nucleotides surrounding the guanine nucleotide are important for the mutation frequency in BaP-treated mice and in BaP-untreated *nrf2*$^{-/-}$ mice.

Several lines of recent evidence have pointed towards a role for Nrf2 in prevention of carcinogenesis. One of the salient examples is that Nrf2 could prevent the formation of DNA adduct and gastric tumors from occurring after BaP administration (10, 11). Furthermore, Nrf2-deficient mice are sensitive to the alkylating agent [*N*-nitrosobutyl(4-hydrixybutyl)amine] and rapidly form bladder tumors after administration (34). This study shows that Nrf2 can prevent increase in the number of spontaneous and inducible mutations that occur in the *gpt* gene in mouse lung and liver and can prevent the induction of mutations at the hotspots, such as nucleotides 64 and 140 in the lung. We surmise that through induction of phase II and antioxidant enzyme activities as well as cross-talk with phase I detoxifying system (35), Nrf2 can mitigate the effects of mutagens, such as BaP, on adduct formation, leading to protection from neoplasm and tumor formation and ultimately aiding in prevention of pulmonary diseases that arise, such as lung cancer from tobacco smoke (36), or from hyperoxic injury (37).

The results presented in this study suggest that Nrf2 deficiency is a possible risk factor for development of lung cancer or other lung diseases caused by mutagens or oxidants in ambient air. Whereas molecular mechanisms by which Nrf2 deficiency changes the mutation profile still require clarification, one plausible explanation is that Nrf2 deficiency may allow accumulation of specific reactive oxygen intermediates or electrophiles. We are now examining how exaggerated mutagenesis in the Nrf2-deficient condition quantitatively contributes to the enhanced carcinogenicity. We believe that the Nrf2-deficient *gpt* delta mice will provide useful information for revealing the relationship between *in vivo* mutagenesis and carcinogenicity.

Acknowledgments

Received 9/18/2006; revised 3/10/2007; accepted 4/9/2007.

Grant support: Japan Society for the Promotion of Sciences grant-in-aid for scientific research 14207100 (Y. Aoki, A.H. Hashimoto, T. Nohmi, and M. Yamamoto) and JST-ERATO (K. Itoh and M. Yamamoto).

The costs of publication of this article were defrayed in part by the payment of page charges. This article must therefore be hereby marked *advertisement* in accordance with 18 U.S.C. Section 1734 solely to indicate this fact.

We thank Dr. John D. Hayes for providing us anti-mouse GST A1/2 and GST A3 antibodies; Dr. Ichiro Hatayama for GST P1/2 antibody; Drs. Hiroaki Shiraishi, Wakae Maruyama, Rie Yanagisawa (National Institute for Environmental Studies), and Jon Maher (University of Tsukuba) for their support and advice; and Yukari Sakashita, Yoshiki Sugawara (National Institute for Environmental Studies), and Katsuyoshi Hayashi (Animal Care Co., Ltd.) for their excellent technical contribution.

References

1. Motohashi H, Yamamoto M. Nrf2-Keap1 defines a physiologically important stress response mechanism. Trends Mol Med 2004;10:549–57.
2. Ishii T, Itoh K, Takahashi S, et al. Transcription factor Nrf2 coordinately regulates a group of oxidative stress-inducible genes in macrophages. J Biol Chem 2000;275: 16023–9.
3. Cho HY, Jedlicka AE, Reddy SP, et al. Role of NRF2 in protection against hyperoxic lung injury in mice. Am J Respir Cell Mol Biol 2002;26:175–82.
4. Tong KI, Kobayashi A, Katsuoka F, Yamamoto M. Two-site substrate recognition model for Keap1-Nrf2 system: a hinge and latch mechanism. Biol Chem 2006; 387:1311–20.
5. Itoh K, Tong KI, Yamamoto M. Molecular mechanism activating Nrf2-Keap1 pathway in regulation of adaptive response to electrophiles. Free Radic Biol Med 2004;36: 1208–13.
6. Kobayashi A, Kang MI, Watai Y, et al. Oxidative and electrophilic stresses activate Nrf2 through inhibition of ubiquitination activity of Keap1. Mol Cell Biol 2006;26: 221–9.
7. Itoh K, Chiba T, Takahashi S, et al. An Nrf2/small Maf heterodimer mediates the induction of phase II detoxifying enzyme genes through antioxidant response elements. Biochem Biophys Res Commun 1997;236: 313–22.
8. Aoki Y, Sato H, Nishimura N, Takahashi S, Itoh K, Yamamoto M. Accelerated DNA adduct formation in the lung of the Nrf2 knockout mouse exposed to diesel exhaust. Toxicol Appl Pharmacol 2001;173:154–60.
9. Enomoto A, Itoh K, Nagayoshi E, et al. High sensitivity of Nrf2 knockout mice to acetaminophen hepatotoxicity associated with decreased expression of ARE-regulated drug metabolizing enzymes and antioxidant genes. Toxicol Sci 2001;59:169–77.
10. Ramos-Gomez M, Kwak MK, Dolan PM, et al. Sensitivity to carcinogenesis is increased and chemoprotective efficacy of enzyme inducers is lost in nrf2 transcription factor-deficient mice. Proc Natl Acad Sci U S A 2001;98:3410–5.
11. Ramos-Gomez M, Dolan PM, Itoh K, Yamamoto M, Kensler TW. Interactive effects of nrf2 genotype and oltipraz on benzo[*a*]pyrene-DNA adducts and tumor yield in mice. Carcinogenesis 2003;24:461–7.
12. Nohmi T, Katoh M, Suzuki H, et al. A new transgenic mouse mutagenesis test system using Spi- and 6-thioguanine selections. Environ Mol Mutagen 1996;28: 465–70.
13. Hashimoto AH, Amanuma K, Hiyoshi K, et al. *In vivo* mutagenesis induced by benzo[*a*]pyrene instilled into the lung of *gpt* delta transgenic mice. Environ Mol Mutagen 2005;45:365–73.
14. Nohmi T, Suzuki T, Masumura K. Recent advances in the protocols of transgenic mouse mutation assays. Mutat Res 2000;455:191–215.
15. Thybund V, Dean S, Nohmi T, et al. *In vivo* transgenic mutation assays. Mutat Res 2003;540:141–51.
16. Chanas SA, Jiang G, McMahon M, et al. Loss of the Nrf2 transcription factor causes a marked reduction in constitutive and inducible expression of the glutathione *S*-transferase *Gsta1, Gsta2, Gstm1, Gstm2, Gstm3* and *Gstm4* genes in the liver of male and female mice. Biochem J 2002;365:405–18.
17. Aoki Y, Satoh K, Sato K, Suzuki KT. Induction of glutathione S-transferase P-form in primary cultured rat liver parenchymal cells by co-planar polychlorinated biphenyl congeners. Biochem J 1992;281:539–43.
18. McLellan LI, Hayes JD. Differential induction of class alpha glutathione *S*-transferases in mouse liver by the anticarcinogenic antioxidant butylated hydroxyanisole. Purification and characterization of glutathione *S*-transferase Ya1Ya1. Biochem J 1989;263:393–402.
19. Hayes JD, Judah DJ, Neal GE, Nguyen T. Molecular cloning and heterologous expression of a cDNA encoding a mouse glutathione *S*-transferase Yc subunit possessing high catalytic activity for aflatoxin B1-8,9-epoxide. Biochem J 1992;285:173–80.
20. Hayes JD, Flangan JU, Jowsey IR. Glutathione transferase. Annu Rev Pharmacol Toxicol 2005;25:51–88.
21. Cariello NF, Piegorsch WW, Adams WT, Skopek TR. Computer program for the analysis of mutational spectra: application to p53 mutations. Carcinogenesis 1994;15:2281–5.
22. Tomascik-Cheeseman LM, Colemana MA, Marchettia F, et al. Differential basal expression of genes associated with stress response, damage control, and DNA repair among mouse tissues. Mutat Res 2004;561:1–14.
23. Buening MK, Wislocki PG, Levin W, et al. Tumorigenicity of the optical enantiomers of the diastereomeric benzo[*a*]pyrene 7,8-diol-9,10-epoxides in newborn mice: exceptional activity of (+)-7beta,8alpha-dihydroxy-9alpha,10alpha-epoxy-7,8,9,10-tetrahydrobenzo[*a*]pyrene. Proc Natl Acad Sci U S A 1978;75:5358–61.
24. Cosman M, de los Santos C, Fiala F, et al. Solution conformation of the major adduct between the carcinogen (+)-anti-benzo[*a*]pyrene diol epoxide and DNA. Proc Natl Acad Sci U S A 1992;89:1914–8.
25. Hakura A, Tsutsui Y, Sonoda J, Tsukidate K, Mikami T, Sagami F. Comparison of the mutational spectra of the *lacZ* transgene in four origins of the Muta Mouse treated with benzo[*a*]pyrene: target organ specificity. Mutat Res 2000;447:239–47.
26. Shane BS, de Boer J, Watson DE, Haseman JK, Glickman BW, Tindall KR. *LacI* mutation spectra following benzo[*a*]pyrene treatment of Big Blue mice. Carcinogenesis 2000;21:715–25.
27. Hanrahan CJ, Bacolod MD, Vyas RR, et al. Sequence specific mutagenesis of the major (+)-anti-benzo[*a*]pyrene diol epoxide-DNA adduct at a mutational hot spot *in vitro* and in *Escherichia coli* cells. Chem Res Toxicol 1997;10:369–77.
28. Chiapperino D, Kroth H, Kramarczuk IH, et al. Preferential misincorporation of purine nucleotides by human DNA polymerase eta opposite benzo[*a*]pyrene 7,8-diol 9,10-epoxide deoxyguanosine adducts. J Biol Chem 2002;277:11765–71.
29. Yoshimoto T, Inoue T, Iizuka H, et al. Differential induction of squamous cell carcinoma and adenocarcinoma on mouse lung by intratracheal instillation of benzo(a)pyrene and charcoal powder. Cancer Res 1980; 40:4301–7.
30. Dreij K, Sundberg K, Johansson AS, et al. Catalytic activities of human alpha class, glutathione transferases toward carcinogenic dibenzo[*a l*]pyrene diol epoxides. Chem Res Toxicol 2002;15:825–31.
31. Arai T, Kelly VP, Komoro K, Minowa O, Noda T, Nishimura S. Cell proliferation in liver of *mmh/ogg1*-deficient mice enhances mutation frequency because of the presence of 8-hydroxyguanine in DNA. Cancer Res 2003;63:4287–92.
32. Srivastava SK, Watkins SC, Schuetz E, Singh SV. Role of glutathione conjugate efflux in cellular protection against benzo[*a*]pyrene-7,8-diol-9,10-epoxide-induced DNA damage. Mol Carcinog 2002;33:156–62.
33. Burdick AD, Davis JW II, Liu KJ, et al. Benzo[*a*]pyrene quinones increase cell proliferation, generate reactive oxygen species, and transactivate the epidermal growth factor receptor in breast epithelial cells. Cancer Res 2003;63:7825–33.
34. Iida K, Itoh K, Kumagai Y, et al. Nrf2 is essential for the chemopreventive efficacy of oltipraz against urinary bladder carcinogenesis. Cancer Res 2004;64:6424–31.
35. Kohle C, Bock KW. Activation of coupled Ah receptor and Nrf2 gene batteries by dietary phytochemicals in relation to chemoprevention. Biochem Pharmacol 2006; 72:795–805.
36. Wenzlaff AS, Cote ML, Bock CH, Land SJ, Schwartz AG. GSTM1, GSTT1 and GSTP1 polymorphisms, environmental tobacco smoke exposure and risk of lung cancer among never smokers: a population-based study. Carcinogenesis 2005;26:395–401.
37. Cho HY, Jedlicka AE, Reddy SP, Zhang LY, Kensler TW, Kleeberger SR. Linkage analysis of susceptibility to hyperoxia. Nrf2 is a candidate gene. Am J Respir Cell Mol Biol 2002;26:42–51.

Genes and Environment, Vol. 29, No. 3 pp. 89-99 (2007)

Regular article

Mutation Spectra in Cisplatin- and Transplatin-treated GDL1 Cells Clarified the Different Mode of Action of These Compounds in Mammalian Cells

Akira Takeiri[1,3], Masayuki Mishima[1], Kenji Tanaka[1], Akifumi Shioda[1], Asako Harada[1], Ken-ichi Masumura[2] and Takehiko Nohmi[2]

[1]Fuji Gotemba Research Laboratories, Chugai Pharmaceutical Co., Ltd., Shizuoka, Japan
[2]Division of Genetics and Mutagenesis, National Institute of Health Sciences, Tokyo, Japan

(Received April 11, 2007; Revised June 6, 2007; Accepted June 15, 2007)

Cisplatin is an active antitumor drug but its stereoisomer, *i.e.*, transplatin, is clinically inactive. We characterized the gene mutations induced by both isomers using cell line GDL1 established from *gpt* delta transgenic mice. Because cisplatin exhibited about 100 times higher cytotoxicity than transplatin, the cells were treated with cisplatin at doses of 0.25, 0.5, and 1 μg/mL and with transplatin at doses of 12.5, 25, and 50 μg/mL for 24 h. After an additional 2- to 8-day culture, mutant frequencies (MFs) with both Spi⁻ and 6-thioguanine (6-TG) selection were determined. In Spi⁻ selection, MFs in cisplatin- or transplatin-treated cells showed an increase of up to twofold that of vehicle-treated cells. A midsize deletion less than 1 kilo base pair (kbp) in size and single base deletions in non-run sequences were significantly induced by treatment with both compounds. In 6-TG selection, MFs increased up to 3.7-fold in the cisplatin-treated cells and 2.6-fold in transplatin-treated cells compared to vehicle-treated cells. Hotspots of cisplatin- and transplatin-induced mutations were found in 5′-NGG-3′, 5′-GGN-3′, and 5′-GNG-3′ sequences (N is the mutated nucleotide) and 5′-GCG-3′, 5′-GCCG-3′, 5′-GCN-3′, and 5′-GGGN-3′ (G, C, or N is the mutated nucleotide), respectively. These findings are consistent with previous reports using cell-free systems that cisplatin induces intrastrand crosslinks between two purine bases in 5′-GG-3′, 5′-AG-3′, and 5′-GNG-3′ and that transplatin primarily forms mono adducts in the guanine bases and needs multiple guanine adducts to form crosslinks. We suggest that intrastrand crosslinks play key roles in the cytotoxicity and mutagenicity induced by these two platinum compounds and that the more efficient formation of intrastrand crosslinks of cisplatin compared to transplatin may account for the potent cytotoxicity and clinical activity. The spectral analysis of mutations using GDL1 cells would provide valuable information on the mechanisms underlying the mutagenesis induced by the platinum stereoisomers.

Key words: cisplatin, transplatin, mutation spectra, *gpt delta* mouse, GDL1 cells, cell line

Introduction

Formation of characteristic DNA adducts, generation of oxidative radical species, disturbance of cellular DNA synthesis, and so forth are known mechanisms for inducing genetic mutation. Induced mutation spectra are reflections of various actions of mutagens on DNA and thus detailed analyses of mutation spectra provide further clarification of the mode of action involved. The *gpt* delta L1 (GDL1) cell line established from *gpt* delta mice is a convenient tool for molecular analyses of mutation spectra (1). The cells carry chromosomally integrated lambda EG10 shuttle vector DNA with the *red/gam* genes and the *gpt* genes of *Escherichia coli* (*E. coli*) that are suitable for easy isolation of mutants and for sequence analysis of induced mutations. Deletion mutations of sizes from 1 base pair (bp) to about 10 kilo base pair (kbp) in the *red/gam* genes and point mutations in the *gpt* gene can be individually identified by sensitive to P2 interference (Spi⁻) selection and 6-thioguanine (6-TG) selection, respectively. We previously detected mutations characteristic of induction by mitomycin C (MMC) in GDL1 cells, which suggested that the cell line would be a useful tool for analyses of mutation spectra (1).

cis-Diamminedichloroplatinum(II) (cisplatin, Fig. 1) is a widely used chemotherapeutic agent in the clinical treatment of tumors, especially in testicular and ovarian cancers (2). The covalent adducts generated by cisplatin in cellular DNA are implicated in the cytotoxicity of the agent (3). However, the agent inevitably has mutagenic property (4–7). Interestingly, *trans*-diamminedichloroplatinum(II) (transplatin, Fig. 1), the stereoisomer of cisplatin, is in contrast to cisplatin with respect to clini-

[3]Correspondence to: Akira Takeiri, Fuji Gotemba Research Labs., Chugai Pharmaceutical Co., Ltd., 1-135 Komakado, Gotemba, Shizuoka 412-8513, Japan. Tel: +81-550-87-6376, Fax: +81-550-87-6383, E-mail: takeiriakr@chugai-pharm.co.jp

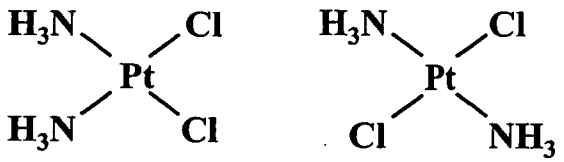

Cisplatin **Transplatin**

Fig. 1. Structure of *cis*-diamminedichloroplatinum(II) (cisplatin) and *trans*- diamminedichloroplatinum(II) (transplatin).

cal efficiency, cytotoxicity, or mutagenicity (8–12). It was reported that transplatin as well as cisplatin forms DNA adducts resulting in genotoxicity (11,13,14). DNA adducts formed by cisplatin or transplatin have been well studied in cell-free systems. Cisplatin binds to guanine and adenine residues in DNA. It forms intrastrand crosslinks in 5′-GG-3′, 5′-AG-3′, and 5′-GNG-3′ sequences or interstrand crosslinks in the 5′-GC-3′ sequence. A majority of cisplatin-induced adducts were intrastrand crosslinks, whereas only 1% of the total DNA adducts were interstrand crosslinks (15,16). On the other hand, transplatin primarily forms monofunctional adducts in guanine residues. The monoadducts subsequently bind to cytosine residues in the complement strand of DNA and generate interstrand crosslinks (17). The conversion of the linkage isomerization from a monofunctional into a bifunctional adduct is relatively slow (17). Therefore, almost all adducts of transplatin are monofunctional, while 10% to 20% of transplatin adducts are interstrand crosslinks (17,18).

The mutation spectra induced by cisplatin were well investigated in *E. coli* (4,6,19,22), mammalian cells (5,21,22) and mice (7). In contrast to the detailed investigations for cisplatin, little is known about mutation spectra induced by transplatin, especially in mammalian cells. The difference in chemotherapeutic or mutagenic activity between these stereoisomers is thought to be related to the different kinetics of the formation of DNA adducts (23,24). However, the difference has been discussed using data obtained from cell-free systems. In order to provide substantial evidence to explain the difference in mutagenicity and cytotoxicity between these compounds, information on the DNA sequence-alteration induced by these compounds in mammalian cells is required.

In the present study, we focused on the genetic mutations induced by two platinum stereoisomers using GDL1 cells. We discussed the differences in the mutation-induction mechanisms of these compounds using mammalian cells.

Materials and Methods

Cytotoxicity: GDL1 cells were cultured in Dulbecco's modified Eagle's medium (DMEM, Sigma-Aldrich, St. Louis, MO, USA) supplemented with 10% (v/v) heat-inactivated fetal bovine serum (FBS, Invitrogen, Carlsbad, CA, USA) in a humidified atmosphere of 5% CO_2 at 37°C. The cells were plated in 12-multiwell culture plates (Corning, Corning, NY, USA) at a density of 2×10^4 cells/mL in each well. One day after plating, the cells were treated with cisplatin (Sigma-Aldrich) at doses of 0.25, 0.5, and 1 μg/mL or with transplatin (Sigma-Aldrich) at doses of 12.5, 25, and 50 μg/mL for 24 h. Solutions of the platinum complexes were freshly prepared with dimethyl sulfoxide (DMSO) and aliquots of the solutions were added to the cell cultures immediately. The cells were harvested after a 24-h culture using trypsin-EDTA treatment and the viable cell numbers were counted using trypan blue (Sigma-Aldrich) staining.

Treatment with cisplatin or transplatin and preparation of lambda EG10 phage: Three culture flasks (25 cm^2, Corning) containing 2×10^5 cells/5 mL were prepared for each dose 1 day before the treatment. The cells were exposed to cisplatin at doses of 0.25, 0.5, and 1 μg/mL or transplatin at doses of 12.5, 25, and 50 μg/mL for 24 h and washed with DMEM. The cells were re-suspended in 10 mL culture medium, transferred into 75-cm^2 culture flasks and subcultured for 2-8 days until confluence. Genomic DNA was extracted using a RecoverEase DNA isolation kit (Stratagene, La Jolla, CA, USA). The lambda EG10 phages were rescued from the genomic DNA by in vitro packaging reaction using Transpack packaging extract (Stratagene) according to the manufacturer's instructions.

Measurement of mutant frequency (MF) and sequence analysis: The lambda EG10 phages were transfected to host bacterial strains. MFs were measured by Spi$^-$ selection and 6-TG selection as described by Nohmi (see the detailed protocol at http://dgm2alpha.nihs.go.jp/dgm2/). The Spi$^-$ mutant phages obtained from Spi$^-$ selection and *gpt* mutant bacterial colonies from 6-TG selection were used for sequence analysis as previously described (25,26). The DNA sequences of the *gam* gene or sequences flanking the deletion junction were analyzed in 48 Spi$^-$ mutants from vehicle-treated cells and 45 Spi$^-$ mutants each from cisplatin (1 μg/mL)- and transplatin (50 μg/mL)-treated cells. The DNA sequence of the *gpt* gene in 49 *gpt* mutants from vehicle-treated cells and 45 *gpt* mutants each from cisplatin (0.5 μg/mL)- and transplatin (50 μg/mL)-treated cells were analyzed. Analysis was performed with a BigDye Terminator Cycle Sequencing Kit (Applied Biosystems, Foster City, CA, USA) and Genetic Analyzer, ABI PRISM 3100 or 3700 (Applied Biosystems). In both *gpt* and Spi$^-$ mutants, the mutations analyzed were classified by type of mutation. The ratio of each type of mutation to total mutations

was multiplied by total MF to determine specific MF. The specific MFs of the chemical-treated cells were statistically compared with those of the control cells using Fisher's exact test according to the method of Carr and Gorelick (27).

Results

Cytotoxicity: The cytotoxicity of cisplatin and transplatin in GDL1 cells is shown in Fig. 2. The approximate IC_{50} of cisplatin was 0.3 μg/mL, whereas that of transplatin was 30 μg/mL. Cisplatin showed 100-fold higher cytotoxicity compared to transplatin.

Mutant frequency in Spi$^-$ selection and 6-TG selection: The Spi$^-$ MF was 14.5×10^{-6} in vehicle-treated cells. Both of the platinum complexes significantly increased the Spi$^-$ MFs up to twofold that of the vehicle-treated cells (Fig. 3). The Spi$^-$ MFs were

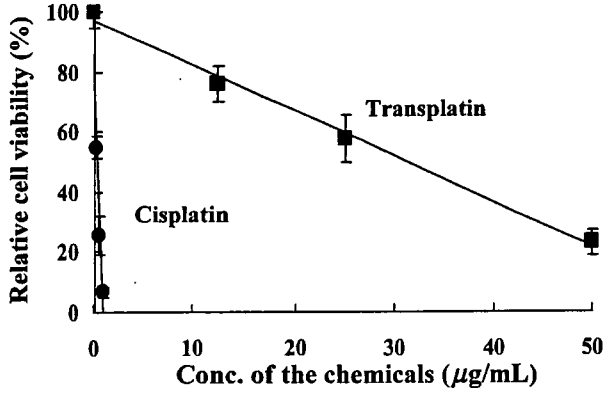

Fig. 2. Cytotoxicity of cisplatin and transplatin in GDL1 cells. The cells were treated, cultured for 24 h, and the number of viable cells determined after an additional 24-h culture.

13.5×10^{-6}, 25.4×10^{-6}, and 28.6×10^{-6} after treatments of 0.25, 0.5, and 1 μg/mL of cisplatin, respectively (Fig. 3A). The Spi$^-$ MFs in transplatin-treated cells were 18.6×10^{-6}, 22.6×10^{-6}, and 29.5×10^{-6} at doses of 12.5, 25, and 50 μg/mL, respectively (Fig. 3B).

The *gpt* MF of vehicle-treated cells was 8.7×10^{-6} (Fig. 4). The *gpt* MFs of cisplatin-treated cells showed a significant increase of up to 3.7-fold that of the vehicle-treated cells (Fig. 4A). Cisplatin increased the *gpt* MFs to 13.2×10^{-6}, 31.9×10^{-6}, and 25.3×10^{-6} at doses of 0.25, 0.5, and 1 μg/mL, respectively. The *gpt* MFs of transplatin-treated cells also significantly increased up to 2.6-fold that of the vehicle-treated cells (Fig. 4B). Transplatin increased the *gpt* MFs to 9.2×10^{-6}, 17.5×10^{-6}, and 22.8×10^{-6} at doses of 12.5, 25, and 50 μg/mL, respectively.

Molecular nature of Spi$^-$ mutations induced by cisplatin and transplatin: The DNA sequences of the Spi$^-$ mutants induced by cisplatin and transplatin were determined. The mutations were categorized into five classes (Table 1) with some subclasses. Specific MFs for each class and subclass were determined by multiplying the percentage of each class of mutants and the total MF. Large deletions more than 1 kbp in deletion size were classified as class I and midsized deletions from 2 bp to 1 kbp were classified as class II. Classes I and II were subclassified according to the existence of microhomology sequence at the deletion junction into A (with microhomology) or B (without microhomology). Single base deletions occurring in the *gam* gene were classified as class III and subclassified according to induction at a run sequence (A) and at a non-run sequence (B) of identical bases. Complex mutations were classified as class IV. Miscellaneous mutations including base substi-

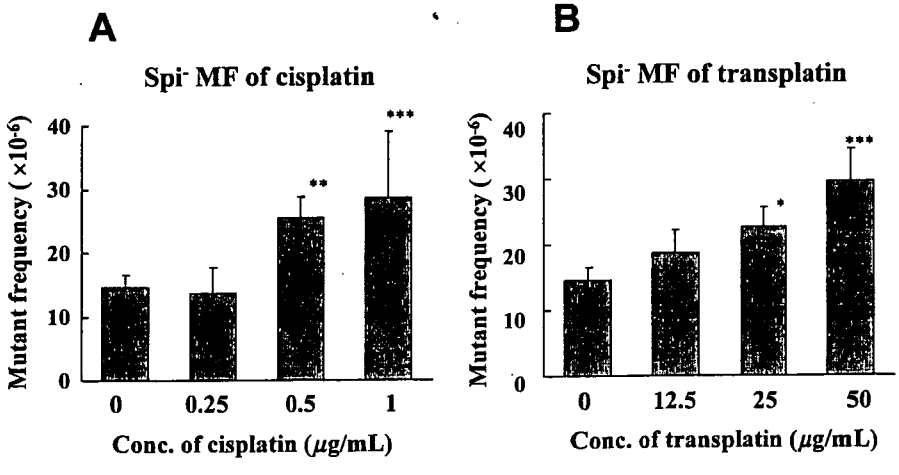

Fig. 3. Spi$^-$ MFs in cisplatin- or transplatin-treated GDL1 cells. (A) Spi$^-$ MF of cisplatin (B) Spi$^-$ MF of transplatin. Cells were treated, cultured for 24 h and harvested after an additional 2- to 8-day culture following the determination of Spi$^-$ MFs with Spi$^-$ selection. P-values calculated by Fisher's exact test were $p<0.01$ (*), $p<0.001$ (**), and $p<0.0001$ (***). Bars represent mean and SD of data obtained from 3 independent cell culture flasks. The MF values compensated by numbers of clonal mutants were 4.8×10^{-6}, 12.1×10^{-6}, and 13.1×10^{-6} in control, cisplatin (1 μg/mL)-treated, and transplatin (50 μg/mL)-treated groups, respectively.

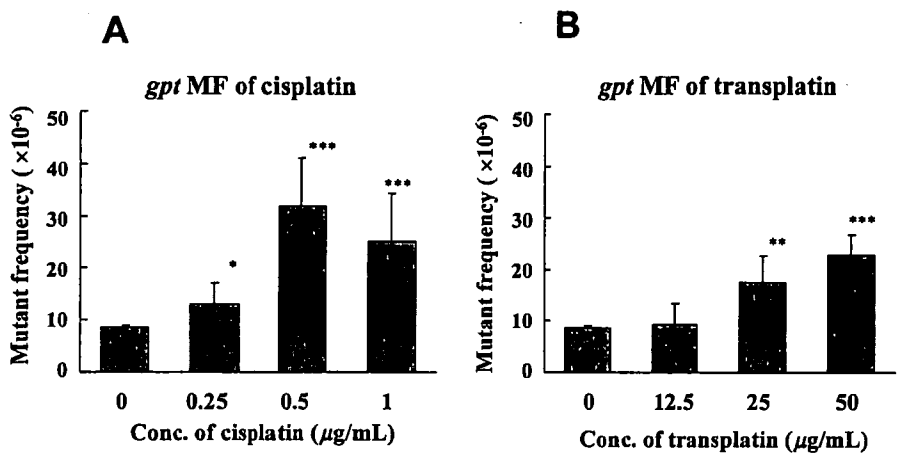

Fig. 4. *gpt* MFs in cisplatin- or transplatin-treated GDL1 cells. (A) *gpt* MF of cisplatin (B) *gpt* MF of transplatin. Cells were treated, cultured for 24 h, and harvested after an additional 2- to 8-day culture following the determination of *gpt* MFs with 6-TG selection. P-values calculated by Fisher's exact test were $p<0.05$ (*), $p<0.01$ (**), and $p<0.0001$ (***). Bars represent mean and SD of data obtained from 3 independent cell culture flasks.

Table 1. Summary of Spi⁻ mutations derived from the GDL1 cells treated with cisplatin and transplatin

Class of mutation	Type of mutation	Control		Cisplatin			Transplatin		
		No. of mutants (%)	Specific MF* ($\times 10^{-6}$)	No. of mutants (%)	Specific MF* ($\times 10^{-6}$)	P value†	No. of mutants (%)	Specific MF* ($\times 10^{-6}$)	P value†
	Large deletion (>1 kbp)								
I-A	with microhomology at the junction	7 (14.6)	2.1	1 (2.2)	0.6	0.28	5 (11.1)	3.3	0.54
I-B	without microhomology at the junction	0 (0.0)	0.0	0 (0.0)	0.0	—	1 (2.2)	0.7	0.32
	Midsize deletion (2 bp − 1 kbp)								
II-A	with microhomology at the junction	1 (2.1)	0.3	4 (8.9)	2.5	<0.05	0 (0.0)	0.0	1.00
II-B	without microhomology at the junction	0 (0.0)	0.0	1 (2.2)	0.6	0.33	8 (17.8)	5.2	<0.0001
	Single base deletion								
III-A	at run sequence	31 (64.6)	9.4	24 (53.3)	15.3	0.12	20 (44.4)	13.1	0.23
III-B	at non-run sequence	0 (0.0)	0.0	4 (8.9)	2.5	<0.05	3 (6.7)	2.0	<0.05
IV	Complex mutation	0 (0.0)	0.0	2 (4.4)	1.3	0.11	0 (0.0)	0.0	—
V	Miscellaneous mutation	9 (18.8)	2.7	7 (15.6)	4.4	0.43	7 (15.6)	4.6	0.29
	Unidentified	0 (0.0)	0.0	2 (4.4)	1.3	0.11	1 (2.2)	0.7	0.32
	Total	48 (100)	14.5	45 (100)	28.6	<0.0001	45 (100)	29.5	<0.0001

*Specific MF was calculated by multiplying the total mutation frequency by the ratio of each type of mutation to the total mutation. †P values compared to the control group were determined using Fisher's exact test according to Carr and Gorelick (27).

tutions in the *gam* gene were classified as class V. The deletion size and location in lambda EG10 gene of Spi⁻ mutations classified as I-A, I-B, II-A, II-B, and IV are shown in Fig. 5.

The specific MFs were statistically compared between control and treated groups. A significant increase in class II-A and class III-B MFs were observed in cisplatin-treated cells. The MF of class II-A was enhanced more than 8-fold by treatment with cisplatin (2.5×10^{-6} versus 0.3×10^{-6}, Table 1). The MF of class III-B was 2.5×10^{-6} while no mutations of this class were observed in vehicle-treated cells. The size of the deletions of class II-A induced by cisplatin were −21 bp, −437 bp, and −512 bp. These mutants had microhomology sequences of 3 bp to 5 bps (Fig. 5). The two −21 bp deletions were considered to be clonal mutations because their size and location were identical. The class III-B mutants induced by cisplatin were two −1G deletions that occurred at the 5′-GCAGAA-3′ sequence of nucleotide 208 in the *gam* gene and two −1C deletions at the 5′-CGCATG-3′ sequence of nucleotide 345 in the *gam* gene. In transplatin-induced mutations, the

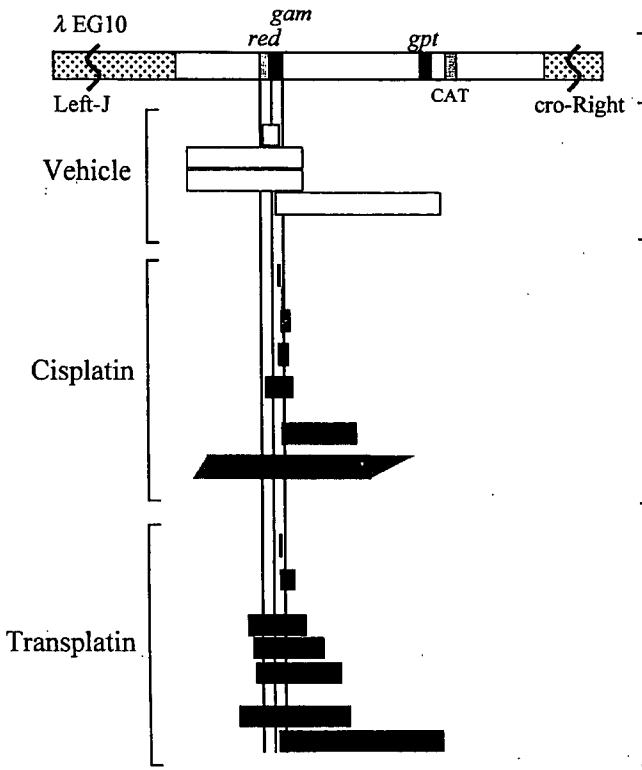

Class	Deletion size	Sequence of deletion junction		No. of mutants	Culture flask ID
II-A	994 bp	CAGCAAAAAATCCAT	CATCACCGCTTCAGA	1	D1
I-A	6827 bp	TTGTTTTTCTGCGGG	GATGAATCCGTCAGT	3	D2
I-A	6827 bp	TTGTTTTTCTGCGGG	GATGAATCCGTCAGT	3	D3
I-A	9792 bp	CGGCGACCGAGTTGC	TGCCAGCGATGCGCA	1	D3
II-A	21 bp	TTCAGGAGCGCATGG	CATGGTTGAAACCAT	2	C3
II-B	157 bp	ATCAAGCAAAAGCAT	AGAAAGAGGCAGAAC	1	C3
II-A	437 bp	TATTGAGCGCAAGAA	AGAACTGGCAGACGA	1	C1
II-A	512 bp	AATTAAGGGAAAATC	ATCCGGTACATGGTT	1	C2
IV	1604 bp deletion and 56 bp insertion	TTGGTTGGGGTAAGC AACTGAAATGCCCGT	GCCTGCTCTCCCGAT CGTACCGGGATCGAT	1	C1
I-A	4380 bp	GTTACAACTGGCAGA	AACTGGCAGACGACA	1	C1
IV	Approx. 9 kbp	ND		1	C2
II-B	139 bp	GATCATTTGCAACGC ^ A	AATGAGTACTGCACT	1	T1
II-B	895 bp	GCCAATGTGCCAATC ^ C	GGTTGAAACCATTGC	7	T3
I-A	3460 bp	GAAGCAGAACGCGCC	CCTCAGCAGGAAAAC	1	T1
I-A	4162 bp	TGATTGACAGCGGAG	GGAGATAAATAATAA	2	T2
I-B	5088 bp	TTGTCACCGGAACGG ^ T	GGCACTGGCTGAAAT	1	T2
I-A	6600 bp	TCGAATCCCTGCCGT	CGTGAAGCGGCAGAG	1	T1
I-A	9792 bp	CGGCGACCGAGTTGC	TGCCAGCGATGCGCA	1	T1

Fig. 5. Deletion mutations classified as I-A, I-B, II-A, II-B, and IV recovered from cisplatin-, transplatin-, and vehicle-treated cells. A partial genetic map of the lambda EG10 transgene, including the *gam* and the *red* target regions of Spi⁻ selection is shown. Horizontal bars represent regions deleted in Spi⁻ mutants. Pointed bar ends denote that the deletion positions were not precisely determined. Junctions are indicated by a space between the left and right sequences. Underlined sequences in the junctions indicate microhomology. One of the two underlined microhomologies at the junctions is deleted when the two DNA fragments are joined. (^) represents the insertion of a sequence in the deletion junction. Culture flasks (3 per group) from which the mutants derived were identified as D1, D2, and D3 for the vehicle (DMSO)-treated flasks; C1, C2, and C2 for the cisplatin-treated flasks, and T1, T2, and to T3 for the transplatin-treated flasks.

Table 2. Summary of *gpt* mutations derived from the GDL1 cells treated with cisplatin and transplatin

Type of mutation	Control		Cisplatin			Transplatin		
	No. of mutants (%)	Specific MF* ($\times 10^{-6}$)	No. of mutants (%)	Specific MF* ($\times 10^{-6}$)	P value†	No. of mutants (%)	Specific MF* ($\times 10^{-6}$)	P value†
Base substitution/Single								
Transition								
G:C→A:T	14 (28.6)	2.5	6 (13.3)	4.3		4 (8.9)	2.0	
A:T→G:C	4 (8.2)	0.7	4 (8.9)	2.8		3 (6.7)	1.5	
Subtotal	18 (36.7)	3.2	10 (22.2)	7.1	0.11	7 (15.6)	3.5	1.00
Transversion								
G:C→T:A	9 (18.4)	1.6	6 (13.3)	4.3		9 (20.0)	4.6	
G:C→C:G	1 (2.0)	0.2	2 (4.4)	1.4		7 (15.6)	3.5	
A:T→T:A	3 (6.1)	0.5	6 (13.3)	4.3		10 (22.2)	5.1	
A:T→C:G	4 (8.2)	0.7	4 (8.9)	2.8		2 (4.4)	1.0	
Subtotal	17 (34.7)	3.0	18 (40.0)	12.8	<0.001	28 (62.2)	14.2	<0.0001
Insertion								
+1A	0 (0.0)	0.0	4 (8.9)	2.8		0 (0.0)	0.0	
+1T	2 (4.1)	0.4	1 (2.2)	0.7		0 (0.0)	0.0	
+1G	0 (0.0)	0.0	0 (0.0)	0.0		0 (0.0)	0.0	
Subtotal	2 (4.1)	0.4	5 (11.1)	3.5	<0.01	0 (0.0)	0.0	1.00
Deletion								
−1A	4 (8.2)	0.7	1 (2.2)	0.7		1 (2.2)	0.5	
−1T	0 (0.0)	0.0	1 (2.2)	0.7		1 (2.2)	0.5	
−1G	1 (2.0)	0.2	0 (0.0)	0.0		2 (4.4)	1.0	
−1C	0 (0.0)	0.0	2 (4.4)	1.4		0 (0.0)	0.0	
>−2 bp	4 (8.2)	0.7	4 (8.9)	2.8		2 (4.4)	1.0	
Subtotal	9 (18.4)	1.6	8 (17.8)	5.7	<0.05	6 (13.3)	3.0	0.25
Base substitution/Tandem								
GA:CT→AG:TC	1 (2.0)	0.2	0 (0.0)	0.0		1 (2.2)	0.5	
TC:AG→GT:CA	0 (0.0)	0.0	1 (2.2)	0.7		0 (0.0)	0.0	
TG:AC→CT:GA	0 (0.0)	0.0	1 (2.2)	0.7		0 (0.0)	0.0	
Subtotal	1 (2.0)	0.2	2 (4.4)	1.4	0.13	1 (2.2)	0.5	0.47
Others	2 (4.1)	0.4	2 (4.4)	1.4	0.21	3 (6.7)	1.5	0.13
Total	49 (100)	8.7	45 (100)	31.9	<0.0001	45 (100)	22.8	<0.0001

*Specific MF was calculated by multiplying the total mutation frequency by the ratio of each type of mutation to the total mutation. †P values were determined using Fisher's exact test according to Carr and Gorelick (27)

MFs of class II-B and class III-B were significantly increased. MF of class II-B deletions was 5.2×10^{-6} and that of class III-B was 2.0×10^{-6} in transplatin-treated cells, whereas no such mutations were induced in vehicle-treated cells. The transplatin-induced class II-B mutations consisted of a −139 bp deletion and −895 bp deletions. Single base insertions with +1A and +1C were respectively induced in the deletion junction of the −139 bp and −895 bp deletions. The seven −895 bp deletions were recognized as clonal mutations, since the deletion size and locus of each were identical. The class III-B mutations included a −1T deletion occurring in the 5′-AGC*T*GGGCG-3′ sequence of nucleotide 163 in *gam* gene, a −1C deletion in the 5′-TGGG*C*GCGT-3′ sequence of nucleotide 167, and a −1C deletion in the 5′-GAATC*G*CTA-3′ sequence of nucleotide 257 in *gam* gene. The −9792 bp deletion in the transplatin-induced mutations was identical to one of the deletions observed in the vehicle-treated cells. Therefore, this deletion formation was not due to the transplatin treatment. In classes I-A, I-B, III-A, IV, and V, no significant increases in specific MF of cisplatin- or transplatin-treated cells were observed. However, sequence analysis demonstrated that the mutants in classes I-A, I-B, and IV of cisplatin- or transplatin-treated cells (with the exception of −9792 bp deletion in transplatin-treated cells) were clearly different in size and location in the lambda EG10 gene compared with the mutants of vehicle-treated cells. These mutants were therefore considered to be induced by the complexes. With regard to the mutants in classes III-A and V, we did not find any characteristic change compared with vehicle-treated cells.

Molecular nature of *gpt* mutations induced by cisplatin and transplatin: The DNA sequence of the *gpt* genes from the 6-TG mutants were determined. The

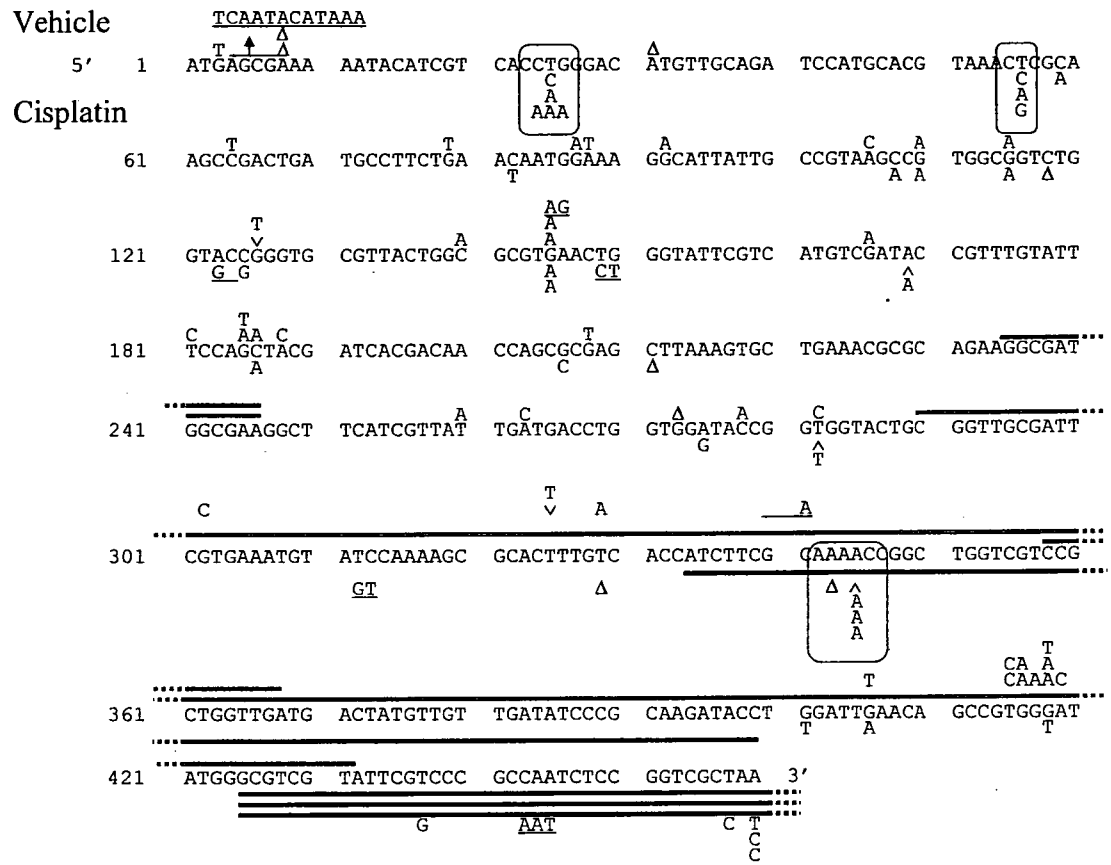

Fig. 6. Mutations in the *gpt* gene from cisplatin- and vehicle-treated GDL1 cells. The sequence from top to bottom represents the coding region of the *gpt* gene. Mutations shown above the sequence are from vehicle-treated cells and below from cisplatin-treated cells. Δ and ∧ represent single base deletions and single base insertion, respectively. Tandem base substitutions and sequence substitutions are underlined. Bars represent deleted sequences in the deletion mutations. Sequences of mutation hot spots are represented by boxes. For cisplatin-treated cells, in 3 of the 506-bp deletions in nucleotides 425 to 930, partial size of the deletions are represented in the figure.

induced mutations were classified, and their specific MFs were calculated and compared with the control values from the vehicle-treated cells (Table 2). After the cisplatin treatment, specific MFs were significantly increased in transversions, insertions, and deletions. Although a statistical significance was not observed, the specific MF of transitions in cisplatin-treated cells exceeded by twofold that of vehicle-treated cells. The MFs of cisplatin-treated cells were increased by 4.3-fold in transversions compared to that of vehicle-treated cells (12.8×10^{-6} vs 3.0×10^{-6}), 8.8-fold in insertions (3.5×10^{-6} vs 0.4×10^{-6}), 3.6-fold in deletions (5.7×10^{-6} vs 1.6×10^{-6}), and 2.2-fold in transitions (7.1×10^{-6} vs 3.2×10^{-6}).

The loci of the mutations in the *gpt* gene induced by cisplatin are shown in Fig. 6. Specific mutations occurred at specific loci that were base substitutions of 5′-CC*T*GG-3′ at nucleotide 25 of the *gpt* gene and of 5′-C*T*C-3′ at nucleotide 56 and single base deletion or insertion of 5′-*AAAA*CC-3′ at nucleotides 342 to 345. The hot spot sequences corresponded to the previously reported 5′-NGG-3′, 5′-GGN-3′, and 5′-GNG-3′ sequences where DNA-cisplatin adducts are favorably formed (15,16). The complementary strand of 5′-CC*T*GG-3′ at nucleotide 25 is 5′-CC*A*GG-3′, also involved in the adduct-favorable sequences. The complementary strand of 5′-*AAAA*CC-3′ at nucleotides 342 to 345 flanked sequence 5′-GGN-3′. We found 27% (12/45) of the cisplatin-induced mutations at these hot spots.

In transplatin-induced *gpt* mutations, the MF of transversions showed a significant increase of 4.7-fold compared to vehicle-treated cells (14.2×10^{-6} vs 3.0×10^{-6}) (Table 2). Transplatin-induced MF of the transversions of G:C to C:G was 18-fold higher (3.5×10^{-6} vs 0.2×10^{-6}), and transversions of A:T to T:A was 10-fold higher (5.1×10^{-6} vs 0.5×10^{-6}) than that of vehicle control. The loci of the mutations induced by transplatin in the *gpt* gene are shown in Fig. 7. Four hot spots were observed. They were 5′-G*C*G-3′ at nucleotide 6, 5′-GCC*G*-3′ at nucleotide 110, 5′-GC*T*-3′ at nucleotide 187, and 5′-GGG*A*-3′ at nucleotide 419 of the *gpt* gene.

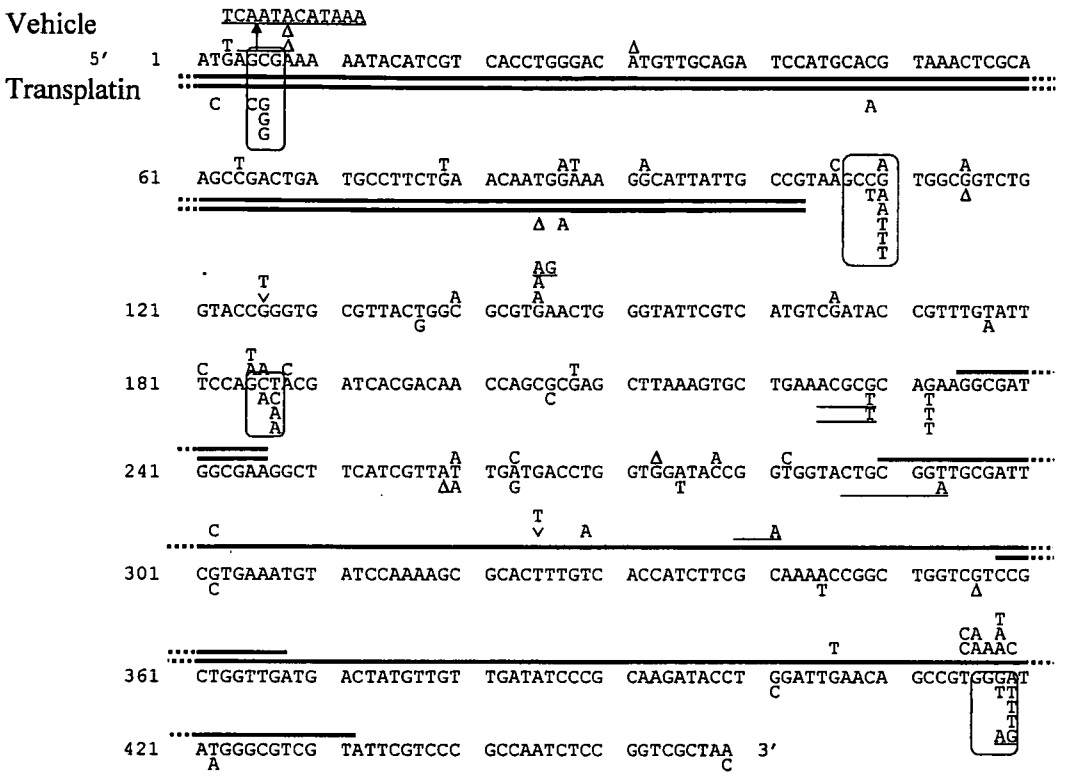

Fig. 7. Mutations in the *gpt* gene from transplatin- and vehicle-treated GDL1 cells detailed in Fig. 6. For transplatin-treated cells, two of the 185-bp deletion in nucleotides −82 to 103 (−82 refers to 82 bp prior to the first base of the first codon) are represented in the figure.

The transplatin hot spots were 5′-GCG-3′, 5′-GCCG-3′, 5′-GCN-3′, and 5′-GGGN-3′. Strict sequence specificity was not observed in transplatin-induced mutations compared to cisplatin-induced mutations. However, all of the mutations induced in the hot spots occurred in the flanking sequence of the G:C rich sequences. The percentage of the total mutations of mutations observed in the hot spots was 42% (19/45).

Discussion

In the present study, cisplatin significantly increased the specific MFs of midsize deletions up to 512 bp (Table 1, Fig. 5). Moreover, cisplatin significantly induced transversions, insertions, and deletions in *gpt* mutants (Table 2). No significant increase was observed in large deletions (classes I-A and IV). However, we concluded that the large deletions were induced by cisplatin because the mutants were unique to cisplatin-treated cells in deletion size and location. Point mutations were predominantly seen in 5′-NGG-3′, 5′-GGN-3′, and 5′-GNG-3′ sequences. Although only minor differences were observed, the mutation spectrum of cisplatin observed in the GDL1 assay system was consistent with the results of the following previous studies. Large deletion mutations less than 9 exons in size were induced in CHO cells (22) and those up to 4 kbp were induced in a TG mouse mutation assay (7). Base substitutions of G:C to T:A, G:C to A:T, and A:T to T:A caused by intrastrand crosslinks at the 5′-AG-3′ or 5′-GG-3′ sequence were observed in *E. coli* (4,19,20,28) and mammalian cells (5,29). Small deletions/insertions and tandem base substitutions were observed in mammalian cells (22). Louro *et al.* reported that base substitutions of G:C to A:T at the 5′-GG-3′ or 5′-AG-3′ sequence and single base deletions/insertions were also seen in cisplatin-treated TG mice (7). These mutations closely correspond to cisplatin-DNA adduct formation observed in cell-free systems (15,16).

Although much attention has been directed to cisplatin-induced mutation spectra, the mutation spectra induced by its stereoisomer transplatin have not been investigated. The present study demonstrated that transplatin significantly induced midsize deletions up to 895 bp (Table 1, Fig. 5) and transversions (Table 2). Although the increase in large deletions (class I-A, I-B) was not statistically significant (Table 1), these large deletions are most likely induced by transplatin because of the characteristic deletion size and loci of the mutants. In transplatin-induced point mutations, base substitutions at 5′-GCG-3′, 5′-GCCG-3′, 5′-GCN-3′, and 5′-GGGN-3′ sequences were dominant. Although transplatin tended to induce mutations at G:C rich sequences, the sequence contexts of the hot spot in transplatin mutagenesis were not as specific as with

cisplatin. Intriguingly, this observation is consistent with the cell-free system as reported by Pinto *et al.* (30) that terminations of DNA synthesis by transplatin occurred in G:C rich sequences and the sequence specificity in the termination regions was more ambiguous compared to that of cisplatin. Pinto *et al.* (30) also showed that the termination of DNA synthesis was caused by crosslinks rather than monoadducts from an experiment using a monofunctional platinum derivative. Bernal-Méndez *et al.* (31) reported the effects of multiple formations of monoadducts on the formation of crosslinks in transplatin using a cell-free system. Multiple monoadducts formed in DNA double strands induce distortion of the strands, which enable the monoadducts to frequently convert into interstrand crosslinks. Since transplatin predominantly forms guanine adducts (17), the induction of mutations in the G:C rich sequences from transplatin observed in the present study is in agreement with the mechanistic understandings of these previous studies. The results of the present study suggest that the DNA adducts detected in cell-free systems contributes to the mutagenesis of transplatin in mammalian cells.

Cisplatin and transplatin produce equal amounts of DNA adducts (10). However, almost all of the cisplatin-induced adducts are crosslinks while the major adducts generated by transplatin are monoadducts (15,16). Furthermore, transplatin requires a much higher concentration compared with cisplatin to produce an equal amount of DNA adducts (9,10). These two factors would contribute to the differences in cytotoxicity between these compounds. With transplatin, a lower reaction rate of the conversion of monoadducts into crosslinks would cause a lower amount of crosslinks (17). Our findings on the differences in mutation spectra induced by cisplatin and transplatin revealed that the different modes of action of these compounds observed in cell-free systems is also observed in mammalian cells.

Cytotoxicity of GDL1 cells from cisplatin was 100 times higher than from transplatin (Fig. 2). The differences in cytotoxicity between cisplatin and transplatin in several mammalian cell lines have been reported. In V79 cells treated for 2 h, cisplatin showed 30- to 40-fold higher cytotoxicity than transplatin (32). In the HeLa cell (33) or Chinese hamster cell (9), cisplatin demonstrated a 5- to 10-fold higher cytotoxicity compared to transplatin. In human ovarian cancer cells, the difference was 70- to 80-fold higher (12). Although the extent of the cytotoxicity depended on test conditions, cisplatin consistently showed higher cytotoxicity than transplatin for all cell lines including GDL1.

Cisplatin has been reported to be more highly mutagenic than transplatin in bacteria (8,13,34). In the reports using mammalian cells, cisplatin showed an apparent increase in MFs but results for transplatin are somewhat contradictory. A slight increase in transplatin-induced MFs were reported in the HGPRT locus of V79 cells (32) or CHO cells (9). Plooy *et al.* (10) reported a clear dose dependent increase of MFs in the *Hprt* locus in CHO cells treated with transplatin. Nishi *et al.* (14) reported that MFs in the *Hprt* locus of V79 cells were obviously increased from transplatin and the MFs induced were equal to those of cisplatin when comparing equitoxic doses. In the present study, the MFs induced by transplatin and cisplatin at equitoxic doses were within a very similar range, consistent with the results of Nishi and his colleagues.

In the cisplatin-treated cells, no significant increase in the specific MF of large deletions (>1 kbp) was observed in the present study, suggesting that the potency of cisplatin in induction of deletions greater than 1 kbp is not high. In our previous study using GDL1 cells, the chemotherapeutic agent mitomycin C (MMC) which generates crosslinks in DNA induced large deletions up to 8 kbp. Almost all crosslinks produced by cisplatin are intrastrand; however, MMC generates both interstrand and intrastrand crosslinks. The difference in crosslinks of these compounds would affect the potency to induce large deletions.

DNA double strand breaks (DSBs) are rejoined at the microhomology sequence with the non-homologous end-joining (NHEJ) which is one of the repair pathways for DSBs in mammalian cells (35). In this study, Spi^- mutant deletions, 7 of 9 (78%) from cisplatin and 5 of 14 (36%) from transplatin, possessed a microhomology sequence of 2 to 10 bp at the deletion junction. These results suggest that at least some of the DSBs induced by these compounds were repaired with NHEJ. Nine of 14 (64%) deletions induced by transplatin were characterized as having no microhomology at the junctions and +1 bp insertions, whereas this type of deletion was not detected from cisplatin treatment (Fig. 5). The difference might be caused by the structural difference in the crosslinks induced by these compounds, *i.e.*, preferential induction of intrastrand crosslinks in cisplatin and interstrand crosslinks in transplatin, and the different types of crosslinks might cause DSBs that are repaired by different mechanisms.

We analyzed mutation spectra induced by cisplatin and transplatin in GDL1 cells. The present study reported a detailed analysis of mutations generated by transplatin for the first time and revealed that the different mutagenic modes of action of the two compounds correlates with their differences in clinical efficiency. Furthermore, the potential utility of the GDL1 assay system in investigations for mutagenesis was shown.

Acknowledgements: This work was supported by a grant-in-aid from the Japan Health Science Foundation (M.I. and T.N.).

References

1 Takeiri A, Mishima M, Tanaka K, Shioda A, Harada A, Watanabe K, Masumura K, Nohmi T. A newly established GDL1 cell line from *gpt* delta mice well reflects the *in vivo* mutation spectra induced by mitomycin C. Mutat Res. 2006; 609: 102-15.

2 Loehrer PJ, Einhorn LH. Drugs five years later. Cisplatin. Ann Intern Med. 1984; 100: 704-13.

3 Rosenberg B. Fundamental studies with cisplatin. Cancer. 1985; 55: 2303-16.

4 Burnouf D, Daune M, Fuchs RP. Spectrum of cisplatin-induced mutations in *Escherichia coli*. Proc Natl Acad Sci USA. 1987; 84: 3758-62.

5 Cariello NF, Swenberg JA, Skopek TR. *In vitro* mutational specificity of cisplatin in the human hypoxanthine guanine phosphoribosyltransferase gene. Cancer Res. 1992; 52: 2866-73.

6 Yarema KJ, Lippard SJ, Essigmann JM. Mutagenic and genotoxic effects of DNA adducts formed by the anticancer drug *cis*-diamminedichloroplatinum(II). Nucleic Acids Res. 1995; 23: 4066-72.

7 Louro H, Silva MJ, Boavida MG. Mutagenic activity of cisplatin in the *lacZ* plasmid-based transgenic mouse model. Environ Mol Mutagen. 2002; 40: 283-91.

8 Plooy AC, Lohman PH. Platinum compounds with antitumour activity. Toxicology. 1980; 17: 169-76.

9 Johnson NP, Hoeschele JD, Rahn RO, O'Neill JP, Hsie AW. Mutagenicity, cytotoxicity, and DNA binding of platinum(II)chloroammines in Chinese hamster ovary cells. Cancer Res. 1980; 40: 1463-8.

10 Plooy AC, van Dijk M, Lohman PH. Induction and repair of DNA crosslinks in Chinese hamster ovary cells treated with various platinum coordination compounds in relation to platinum binding to DNA, cytotoxicity, mutagenicity, and antitumor activity. Cancer Res. 1984; 44: 2043-51.

11 Gebel T, Lantzsch H, Plessow K, Dunkelberg H. Genotoxicity of platinum and palladium compounds in human and bacterial cells. Mutat Res. 1997; 389: 183-90.

12 Pestell KE, Hobbs SM, Titley JC, Kelland LR, Walton MI. Effect of p53 status on sensitivity to platinum complexes in a human ovarian cancer cell line. Mol Pharmacol. 2000; 57: 503-11.

13 Lantzsch H, Gebel T. Genotoxicity of selected metal compounds in the SOS chromotest. Mutat Res. 1997; 389: 191-7.

14 Nishi Y, Hasegawa MM, Taketomi M, Ohkawa Y, Inui N. Comparison of 6-thioguanine-resistant mutation and sister chromatid exchanges in Chinese hamster V79 cells with forty chemical and physical agents. Cancer Res. 1984; 44: 3270-9.

15 Eastman A. Characterization of the adducts produced in DNA by *cis*-diamminedichloroplatinum(II) and *cis*-dichloro(ethylenediamine)platinum(II). Biochemistry. 1983; 22: 3927-33.

16 Eastman A. Reevaluation of interaction of *cis*-dichloro(ethylenediamine)platinum(II) with DNA. Biochemistry. 1986; 25: 3912-5.

17 Brabec V, Leng M. DNA interstrand crosslinks of *trans*-diamminedichloroplatinum(II) are preferentially formed between guanine and complementary cytosine residues. Proc Natl Acad Sci USA. 1993; 90: 5345-9.

18 Boudvillain M, Dalbiès R, Aussourd C, Leng M. Intrastrand crosslinks are not formed in the reaction between transplatin and native DNA: relation with the clinical inefficiency of transplatin. Nucleic Acids Res. 1995; 23: 2381-8.

19 Brouwer J, van de Putte P, Fichtinger-Schepman AM, Reedijk J. Base-pair substitution hotspots in GAG and GCG nucleotide sequences in *Escherichia coli* K-12 induced by *cis*-diamminedichloroplatinum (II). Proc Natl Acad Sci USA. 1981; 78: 7010-4.

20 Burnouf D, Gauthier C, Chottard JC, Fuchs RP. Single d (ApG) / *cis* - diamminedichloroplatinum (II) adduct-induced mutagenesis in *Escherichia coli*. Proc Natl Acad Sci USA. 1990; 87: 6087-91.

21 Bubley GJ, Ashburner BP, Teicher BA. Spectrum of *cis*-diamminedichloroplatinum(II)-induced mutations in a shuttle vector propagated in human cells. Mol Carcinog. 1991; 4: 397-406.

22 Silva MJ, Costa P, Dias A, Valente M, Louro H, Boavida MG. Comparative analysis of the mutagenic activity of oxaliplatin and cisplatin in the *Hprt* gene of CHO cells. Environ Mol Mutagen. 2005; 46: 104-15.

23 Roberts JJ, Friedlos F. Differential toxicity of *cis*- and *trans*-diamminedichloroplatinum(II) toward mammalian cells: lack of influence of any difference in the rates of loss of their DNA-bound adducts. Cancer Res. 1987; 47: 31-6.

24 Chu G. Cellular responses to cisplatin. The roles of DNA-binding proteins and DNA repair. J Biol Chem. 1994; 269: 787-90.

25 Masumura K, Kuniya K, Kurobe T, Fukuoka M, Yatagai F, Nohmi T. Heavy-ion-induced mutations in the *gpt* delta transgenic mouse: Comparison of mutation spectra induced by heavy-ion, X-ray, and gamma-ray radiation. Environ Mol Mutagen. 2002; 40: 207-15.

26 Takeiri A, Mishima M, Tanaka K, Shioda A, Ueda O, Suzuki H, Inoue M, Masumura K, Nohmi T. Molecular characterization of mitomycin C-induced large deletions and tandem-base substitutions in the bone marrow of *gpt* delta transgenic mice. Chem Res Toxicol. 2003; 16: 171-9.

27 Carr GJ, Gorelick NJ. Mutational spectra in transgenic animal research: data analysis and study design based upon the mutant or mutation frequency. Environ Mol Mutagen. 1996; 28: 405-13.

28 Yarema KJ, Wilson JM, Lippard SJ, Essigmann JM. Effects of DNA adduct structure and distribution on the mutagenicity and genotoxicity of two platinum anticancer drugs. J Mol Biol. 1994; 236: 1034-48.

29 de Boer JG, Glickman BW. Sequence specificity of mutation induced by the anti-tumor drug cisplatin in the CHO *aprt* gene. Carcinogenesis. 1989; 10: 1363-7.

30 Pinto AL, Lippard SJ. Sequence-dependent termination of *in vitro* DNA synthesis by *cis*- and *trans*-diamminedichloroplatinum(II). Proc Natl Acad Sci USA. 1985; 82: 4616-9.

31 Bernal-Méndez E, Boudvillain M, González-Vílchez F, Leng M. Chemical versatility of transplatin monofunc-

tional adducts within multiple site-specifically platinated DNA. Biochemistry. 1997; 36: 7281–7.

32 Zwelling LA, Bradley MO, Sharkey NA, Anderson T, Kohn KW. Mutagenicity, cytotoxicity and DNA cross-linking in V79 Chinese hamster cells treated with *cis*- and *trans*-Pt(II) diamminedichloride. Mutat Res. 1979; 67: 271–80.

33 Pascoe JM, Roberts JJ. Interactions between mammalian cell DNA and inorganic platinum compounds. II. Interstrand crosslinking of isolated and cellular DNA by platinum(IV) compounds. Biochem Pharmacol. 1974; 23: 1345–57.

34 Ohta T, Ohmae S, Yamaya K, Kanemichi Y, Tokishita S, Yamagata H. Characterization of the mutational specificity of DNA crosslinking mutagens by the Lac$^+$ reversion assay with *Escherichia coli*. Teratog Carcinog Mutagen. 2001; 21: 275–82.

35 Hefferin ML, Tomkinson AE. Mechanism of DNA double-strand break repair by non-homologous end joining. DNA Repair. 2005; 4: 639–48.

New Insight into Intrachromosomal Deletions Induced by Chrysotile in the *gpt* delta Transgenic Mutation Assay

An Xu,[1,2] Lubomir B. Smilenov,[1] Peng He,[1] Ken-ichi Masumura,[3] Takehiko Nohmi,[3] Zengliang Yu,[2] and Tom K. Hei[1,4]

[1]Center for Radiological Research, College of Physicians & Surgeons, Columbia University, New York, New York, USA; [2]Key Laboratory of Ion Beam Bioengineering, Institute of Plasma Physics, Chinese Academy of Sciences, Hefei, Anhui, People's Republic of China; [3]Division of Genetics and Mutagenesis, National Institute of Health Sciences, Tokyo, Japan; [4]Department of Environmental Health Sciences, Mailman School of Public Health, Columbia University, New York, New York, USA

BACKGROUND: Genotoxicity is often a prerequisite to the development of malignancy. Considerable evidence has shown that exposure to asbestos fibers results in the generation of chromosomal aberrations and multilocus mutations using various *in vitro* approaches. However, there is less evidence to demonstrate the contribution of deletions to the mutagenicity of asbestos fibers *in vivo*.

OBJECTIVES: In the present study, we investigated the mutant fractions and the patterns induced by chrysotile fibers in *gpt* delta transgenic mouse primary embryo fibroblasts (MEFs) and compared the results obtained with hydrogen peroxide (H_2O_2) in an attempt to illustrate the role of oxyradicals in fiber mutagenesis.

RESULTS: Chrysotile fibers induced a dose-dependent increase in mutation yield at the *redBA/gam* loci in transgenic MEF cells. The number of λ mutants losing both *redBA* and *gam* loci induced by chrysotiles at a dose of 1 μg/cm^2 increased by > 5-fold relative to nontreated controls ($p < 0.005$). Mutation spectra analyses showed that the ratio of λ mutants losing the *redBA/gam* region induced by chrysotiles was similar to those induced by equitoxic doses of H_2O_2. Moreover, treatment with catalase abrogated the accumulation of γ-H2AX, a biomarker of DNA double-strand breaks, induced by chrysotile fibers.

CONCLUSIONS: Our results provide novel information on the frequencies and types of mutations induced by asbestos fibers in the *gpt* delta transgenic mouse mutagenic assay, which shows great promise for evaluating fiber/particle mutagenicity *in vivo*.

KEY WORDS: chrysotile asbestos, *gpt* delta transgenic mutation system, kilobase-sized mutation, oxyradicals, γ-H2AX. *Environ Health Perspect* 115:87–92 (2007). doi:10.1289/ehp.9425 available via *http://dx.doi.org/* [Online 6 September 2006]

Asbestos fibers, a group of naturally occurring silicate minerals, are well-established human carcinogens. They are causally related to the development of asbestosis, bronchial carcinoma, malignant mesothelioma of the pleura and peritoneum, and possibly cancers of the gastrointestinal tract and larynx (Gustavsson et al. 1998; International Agency for Research on Cancer 1987). Although the main concern of asbestos-related diseases focuses primarily on the workplace, the danger of developing such diseases now extends beyond that of a simple occupational hazard because accumulating evidence suggests that asbestos fibers are widely distributed in the environment to which the general public may be exposed (Gardner and Saracci 1989). Individuals may be subjected to prolonged exposure to asbestos in their homes, schools, drinking water, neighborhoods of industrial sources of asbestos, or areas of a natural occurring asbestos (Kjaerheim et al. 2005; Miller 2005; Rom et al. 2001). Recent evidence indicates an excess risk of mesothelioma in individuals living in the vicinity of a natural occurring source of asbestos (Pan et al. 2005). The continued discovery of routes through which the general public may be exposed to asbestos suggests a long-term, low-level exposure of a large number of people, which may lead to an elevated risk of asbestos-related diseases.

The mechanisms by which asbestos produces malignancy are unclear at present. It has been reported that fiber dimension, biopersistence, composition, surface reactivity, and physical durability are important criteria for the carcinogenicity of the fibers, indicating that carcinogenic mechanisms of asbestos are likely to be complex and involve multiple pathways (Bernstein et al. 2003; Coin et al. 1994). Various highly quantitative genotoxicity assays ranging from DNA strand breaks to gene mutations in rodent cells have been performed to estimate the carcinogenic potential of asbestos fibers (Lezon-Geyda et al. 1996; Poser et al. 2004). Although asbestos fibers have been shown to induce chromosomal aberrations and sister chromatid exchanges, mutagenic studies at the hypoxanthine–guanine phosphoribosyl transferase (*hprt*; GenBank accession no. NM_013556; http://www.ncbi.nlm.nih.gov/) and ouabain loci in mammalian cells have been shown to be either inactive or weakly active (Jaurand 1996). Using the human–hamster hybrid cell line (A_L) in which mutations are scored at a marker gene (*CD59*) located on human chromosome 11 (11p13) that the A_L cell carries as its only human chromosome, our previous studies have demonstrated that asbestos fibers are indeed mutagenic and induce mostly deletions involving millions of base pairs (Hei et al. 1992). In contrast, among the same fiber-treated A_L cell population, there are few, if any, mutations scored at the *hprt* locus of the hamster X chromosome. This discrepancy has been attributed to the possibility that the *hprt* gene is located on the X chromosome, and large deletions in the region of the gene that are required for cell survival would be lethal and any mutants induced would not be viable. In recent years several other mutagenic assays that are proficient in detecting either large deletions, homologous recombinations, or score mutants located in nonessential genes have been used successfully to demonstrate the mutagenic potential of various fiber types (Lezon-Geyda et al. 1996; Park and Aust 1998). These findings provide a direct link between chromosomal abnormalities that frequently have been demonstrated in fiber exposed human and rodent cell lines and carcinogenicity *in vivo*. However, there is less direct evidence that illustrates chromosomal mutations of asbestos fibers in various organs and tissues in intact organisms.

The use of transgenic mouse systems carrying bacterial reporter genes such as *lacZ*, *lacI*, and *cII* has opened a promising opportunity for short-term mutagenicity analysis (Dean et al. 1999). There is evidence to show that asbestos fibers are mutagenic and induce point mutations in either Big Blue transgenic mice or rats bearing λ-*lacI* as a reporter gene (Rihn et al. 2000; Topinka et al. 2004; Unfried et al. 2002). However, most genome-wide mutations such as large deletions, insertions, translocations, and aneuploidy are not effectively recovered by the *lacI* shuttle vector. To efficiently recover large deletions *in vivo*, *gpt* (xanthine phosphoribosyltransferase;

Address correspondence to T.K. Hei, Center for Radiological Research, Columbia University, New York, NY 10032 USA. Telephone: (212) 305-8462. Fax: (212) 305-3229. E-mail: TKH1@Columbia.edu

We thank M. Partridge and V. Ivanov for their critical reading of the manuscript and R. Baker for his technical assistance with Spi$^-$ detection.

Work was supported in part by National Institutes of Health grant ES 05786, Superfund grant ES 10349, National Institute of Environmental Health Sciences Center grant ES 09089, and National Nature Science Foundation of China grant 20322202.

The authors declare they have no competing financial interests.

Received 14 June 2006; accepted 6 September 2006.

GenBank accession no. NP_414773; http://www.ncbi.nlm.nih.gov/GenBank) delta transgenic mice have been established by integrating multiple copies of λ EG10 DNA with the *redBA* and *gam* (Genbank accession no. J02459; http://www.ncbi.nlm.nih.gov/GenBank) genes into each chromosome 17 of C57BL/6J mice (Nohmi and Masumura 2004). Because wild-type λ-phage DNA replicate poorly in the presence of P2 lysogens in the host cells (called "sensitive to P2 interference" or "Spi"), only mutant λ phages that are deficient in the functions of both the *redBA* and *gam* genes are able to escape from P2 interference (called "Spi$^-$") and form visible clear plaques on a bacterial lawn. Simultaneous inactivations of both the *redBA* and *gam* genes, an indication of deletions in the gene loci region, provide an available method to quantify deletion mutations induced by various physical and chemical mutagens, such as X rays and alkylating agents (Horiguchi et al. 2001; Shibata et al. 2005).

Chrysotile asbestos, a fibrous serpentine, is the most commercially used form of asbestos in the world trade and accounts for > 95% of asbestos found in United States buildings. In the present study we adapted the *gpt* delta transgenic mouse mutation system to evaluate the genotoxicity of chrysotile in *gpt* delta mouse primary embryo fibroblast (MEF) cells. We investigated the mutation frequencies at both *redBA* and *gam* (GenBank accession no. J02459; http://www.ncbi.nlm.nih.gov/GenBank) loci and the contribution of deletions > 2 kb to the mutagenicity of chrysotile fibers. Because reactive oxygen species (ROS) such as superoxide anions (O_2^-) and hydrogen peroxide (H_2O_2) originate not only from redox reactions catalyzed on the fiber surface but also from the incomplete phagocytosis of fibers in various cells, such as phagocytic, mesothelial, and rat lung epithelium cells, we speculated that asbestos fibers would induce similar types of mutations as that of chemically generated oxyradicals. We found that both chrysotile and H_2O_2 dramatically increased the mutation yield, which could be abrogated by concurrent treatment with catalase. Furthermore, the ratios of mutants with deletions > 2 kb were similar to those generated by oxyradicals at two equitoxic doses. The accumulation of phosphorylated histone H2AX (γ-H2AX) further demonstrated the involvement of DNA double-strand break (DSB) in the mutagenicity of chrysotiles. These results provide direct evidence that asbestos fibers induced kilobase pair deletion mutations in a transgenic mouse mutation system, and that these were mediated by oxyradicals.

Materials and Methods

MEF cell culture. *gpt* delta transgenic mice, obtained from T. Nohmi, were mated, and pregnant females were sacrificed on day 14 of the experimental protocol were previously approved by the Columbia University Institutional Animal Care and Use Committee. The animals were treated humanely and with regard for the alleviation of pain and suffering. The embryos were surgically removed and embryonic tissue prepared in culture according to standard procedures (Hogan et al. 1994). These cultures were grown and maintained in Dulbecco's modified Eagle's medium (Gibco-BRL, Gaithersburg, MD, USA) containing 15% heat-inactivated fetal bovine serum and penicillin (100 U/mL), streptomycin (50 μg/mL) in a 5% CO_2 environment at 37°C.

Chrysotile preparation. We used International Union Against Cancer standard reference chrysotile asbestos (average length, 7.8 μm; average diameter, 0.2 μm) in these studies (Timbrell 1979). The fibers were prepared as described previously (Hei et al. 1992). Briefly, samples of fibers were weighed and suspended in distilled water. The fiber suspension was triturated 6–8 times with a 20-gauge syringe needle. A stock solution of the fibers was sterilized by autoclaving and mixed to ensure a uniform suspension before being diluted with tissue culture medium for cell treatment.

Cytotoxicity assay. We evaluated cell viability using MTT (3-(4,5-dimethylthiazol-2-yl)-2,5-diphenyltetrazolium bromide) assay on the basis of the ability of viable cells to convert a water-soluble tetrazolium salt into a water-insoluble formazan product (Scudiero et al. 1988). The enzymatic reduction of the tetrazolium salt happens only in living, metabolically active cells but not in dead cells. Cultures were incubated in two-well chamber slides at a density of 1.0×10^5 cells per well at 37°C for 24 hr. Graded doses of either chrysotile or H_2O_2 were added to the culture medium and incubated for another 24 hr in the presence of serum (chrysotile) or 15 min in the absence of serum (H_2O_2). At the end of the treatment period, the medium was removed, 200 μL of 5 mg/mL MTT was added to each well, and the cultures were incubated for another 4 hr. The supernatant was removed and 1 mL acidic isopropanol was added to dissolve the formazan crystals. The absorbance at 570 nm was determined by an Ultrospec 3100 pro UV/Visible spectrophotometer (Biochrom Ltd., Cambridge, UK).

Genomic DNA isolation. We isolated genomic DNA from MEF cells using the RecoverEase DNA isolation kit (Stratagene, La Jolla, CA, USA) according to the protocol developed by the supplier. Briefly, about 5.0×10^6 cells were transferred to a chilled Wheaton dounce tissue grinder (Fisher, Hampton, NH, USA), and the homogenate obtained was filtered and centrifuged at $1,100 \times g$ for 12 min at 4°C. The pellet was resuspended in digestion buffer containing RNAses (RANse-It; Stratagene) containing proteinase K solution (2 mg/mL prewarmed to 50°C). Using wide-bore pipette tips, the samples were transferred to dialysis cups floating on the surface of TE buffer (500 mL) and dialyzed for 24 hr. The purity and concentration of DNA was checked spectrophotometrically and samples were diluted with TE [10 mM Tris–Cl (pH 7.5), 1 mM EDTA] buffer to a final DNA concentration of approximately 0.5 mg/mL, and stored at 4°C for up to 3 months prior to mutation analysis.

In vitro *packaging of DNA.* The λ DNA was recovered from approximately 5 μg genomic DNA and packaged with terminase and phage proteins contained in the Transpack kit (Stratagene) to produce infectious λ phages. Viable phages were infected into *Escherichia coli* XL-1 Blue MRA (Stratagene), mixed with λ-trypticase agarose and poured onto 100-mm plates containing 30 mL bottom agar. Plates were incubated overnight at 37°C. The average of rescued phages per packaging reaction was 1.8×10^6 in the present studies. There was no significant difference in the titers between control and exposed groups.

Spi$^-$ mutation analysis. The mutant frequencies at *red/gam* loci were determined by Spi$^-$ selection as described previously (Nohmi and Masumura 2004; Nohmi et al. 1996; Shibata et al. 2005). Briefly, packaged phages were infected into *E. coli* XL-1 Blue MRA (P2) (Stratagene). Infected cells were mixed with molten soft agar, poured onto λ-trypticase agar plates and incubated at 37°C. The plaques detected on the plates (Spi$^-$ candidates) were suspended in 50 μL of SM buffer [0.58% NaCl, 0.2% $MgSO_4 \cdot 7H_2O$, 50 mM Tris–HCl, 0.01% gelatin (pH 7.5)]. The suspension was spotted on the two types of plates where *E. coli* XL-1 Blue MRA (P2) or WL95 (P2) strain was spread. The plates were incubated for 24 hr at 37°C. The numbers of mutants that made clear spots on both strains

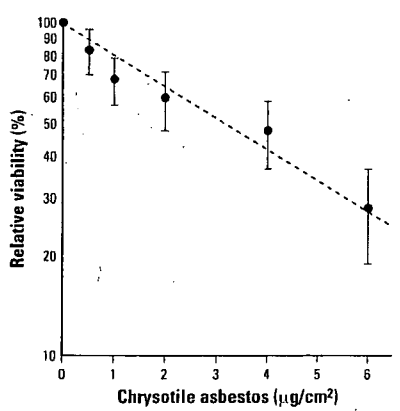

Figure 1. Cell viability of transgenic MEF cells treated with graded doses of chrysotile for 24 hr. Data were the average of three independent experiments. Error bars indicate ± SD.

were counted as confirmed Spi⁻ mutants. Mutation frequencies were calculated by comparing the titration and number of confirmed mutant plaques.

Spi⁻ mutant characterization. To determine the mutated region, the phage DNA was used and subjected to DNA sequence and polymerase chain reaction (PCR) analysis with various sets of primers (Horiguchi et al. 2001). The PCR primers used were as follows: primer 1: 5′-CACTCTCTTT GATGCGAATGCCAGCGTCAGAC-3′; primer 2: 5′-CAGGAGTAATTATGCG GAACAGAATCATGCCTGGTG-3′; primer 3: 5′-GTGAGGATGCGTCATCGCCAT TGCTCCCC-3′; primer 4: 5′-GCGATGA AAAGATGTTTCGTGAAGCCGTC GACGC-3′; primer 5: 5′-AAACAGGCG CGGGCATCAGCGTGGTCTGA-39′; primer 12: 5′-CGCGCGGTCGAGGGACC TAATAACTTCGTA-3′. We performed PCR amplification under the following conditions: 4 µL of phage DNA, 0.2 mM each dNTP, 1.5 mM $MgCl_2$, Taq DNA polymerase (or ExTaq; Takara Shuzo Co., Kyoto, Japan), and 20 pmol of each primer in a 40-µL reaction volume; heating for 1–2 min at 94°C, and 24 cycles at 98°C for 20 sec and at 68°C for X minutes (1 min/1 kb), followed by final extension at 72°C for 10 min. The products were analyzed using agarose gel electrophoresis.

The PCR products were sequenced by ABI's 3100 capillary sequencers (Dye Terminator Cycle Sequencing; PE Applied Biosystems, Foster City, CA, USA). PCR products for templates of sequence were purified using PCR product presequencing kit (Amersham Life Science, Piscataway, NJ, USA).

Sequence primers are as follows: s102: 5′-AATCCAAACTCTTTACCCGTCCTT GGGT-3′; s201: 5′-CGCTTGATAACTCT GTTGAATGGCTCT-3′; s301: 5′-GGTGG AATCCCATCAGCGTTACCGTTT-3′; s302: 5′-AGTGATTGCGCCTACCCG GATATTATCGTG-3′; s403: 5′-CCAGC CGACACGTTCAGCCAGCTTCCCAG-3′. The entire DNA sequence of λ EG10 is available at http://dgm2alpha.nihs.go.jp (Masumura et al. 2003).

Determination of H2AX phosphorylation using flow cytometry. The cells were fixed by adding 2% paraformaldehyde dropwise while being vortexed. The fixed cells were then stained with mouse monoclonal anti–γ-H2AX (Upstate, Lake Placid, NY, USA) and fluorescein isothiocyanate (FITC)–conjugated secondary antibodies (Sigma-Aldrich Chemical Co., St. Louis, MO, USA) as described by Kurose et al. (2005). The cells were then suspended in 0.5 mL of 10 µg/mL propidium iodide (PI) and 40 µg/mL RNase A and incubated at 4°C for at least 30 min. The fluorescence of PI and FITC of individual cells induced by excitation with a 488-nm argon ion laser was measured using a FACSCalibur cytometer (BD Biosciences, San Jose, CA).

Statistical analysis. All numerical data were calculated as mean and SD and evaluated by Student's *t*-test. The statistical significance was tested at $p < 0.05$ as the critical value.

Results

Chrysotile-induced dose-dependent toxicity in transgenic MEF cells. The viability of MEF cells exposed to graded doses of chrysotile was analyzed by using the MTT assay. As shown in Figure 1, exposure of MEF cells to doses of chrysotiles ranging from 0.5 to 6 µg/cm² for 24 hr produced a dose-dependent decrease in cell viability. The viabilities of MEF cells was reduced by 14, 29, and 59%, when the concentrations of chrysotile were 0.5, 1, and 2 µg/cm², respectively. The median lethal dose of chrysotile, which resulted in 50% cell killing, was approximately 3.2 µg/cm².

Mutation frequencies at red/gam *gene loci were elevated in response to chrysotile exposure.* We have shown previously that asbestos is mutagenic and induces multilocus deletions in mammalian cells (Hei et al. 1992). To investigate the mutagenicity of asbestos in the *gpt* delta assay, we used an Spi⁻ mutation assay to determine the mutation frequencies induced by chrysotile exposure in transgenic MEF cells. The average number of spontaneous *red/gam* gene mutants per 10^6 recovered plaques in MEF cells used for these experiments was 4.69 ± 1.80. Treatment of MEF cells with chrysotile fibers resulted in a dose-dependent induction of mutation yield at the *red/gam* gene locus (Figure 2). A significant increase in mutation yield over the background level was observed at fiber concentrations > 1 µg/cm² ($p < 0.005$). The mutant fraction in cells treated with a dose of 1 µg/cm² of fibers was 2.4-fold higher than background. These results indicated that chrysotile asbestos were able to produce deletion mutations in *gpt* delta transgenic mutation assay system.

Characterization of mutant spectra induced by chrysotile. To determine the spectrum of mutations induced by chrysotile fibers, 93 and 74 λ mutants from control cells and cells treated with chrysotile at 1 µg/cm², respectively, were subjected to either PCR analysis or DNA sequence analysis. The PCR product of *redBA/gam* in the wild-type λ EG10 was approximately 2 kb. If a PCR product did not show any discrete alteration on the gel, the mutant was classified as one containing a point mutation with either a base substitution or a frameshift causing no alteration in the size of the gene product. In contrast an absence of visible PCR product was taken as evidence of a mutant with a deletion > 2 kb as a result of losing both *redBA* and *gam* genes. The types of mutations identified from analysis of these mutants are listed in Table 1 and Figure 3. To minimize the possibility that these isolated mutants were spontaneously derived, we

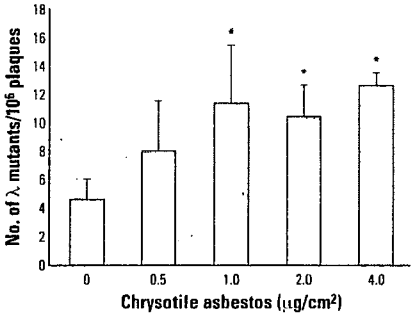

Figure 2. Mutagenic potential of chrysotile asbestos at *redBA* and *gam* loci in transgenic MEF cells. MEF cells, 5 × 10^5, were treated with graded doses of chrysotile as described in the text. Results were expressed as the total number of confirmed λ mutants divided by the total number of rescued phages. The average number of preexisting mutants per 10^6 plaques used for these experiments was 4.69 ± 1.42. Data were pooled from six independent experiments. Error bars indicate ± SD.
*Significantly different at $p < 0.05$.

Table 1. Type of λ-phage mutants at *redBA/gam* loci either of spontaneous origin or induced by chrysotile treatments (1 µg/cm²) determined by multiplex PCR analyses and DNA sequencing.

Groups	Total no. of mutants	No. of mutants with base substitution	No. of mutants with 1-bp deletion	No. of mutants with > 2-bp and < 1-kb deletions	No. of mutants with > 2-kb deletion
Control	93	7 (8%)	68 (73%)	8 (8%)	10 (11%)
Chrysotile	74	5 (7%)	41 (56%)	10 (14%)	17 (23%)

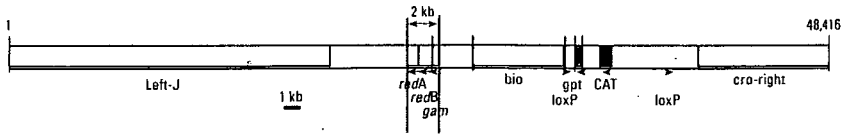

Figure 3. Schematic map of λ EG10 transgene. Abbreviations: bio, genetic marker used in bacteriophage lambda vectors; *CAT*, chloramphenicol acetyltransferase (GenBank accession no. AJ401050; http://www.ncbi.nlm.nih.gov/GenBank/); cro, transcription inhibitor; *gpt*, xanthine phosphoribosyltransferase (GenBank accession no. NP_414773); J, codes for phage tail gene; loxP, locus of X over P1, a site on the bacteriophage P1 consisting of 34 bp; *redA*, *redB*, and *gam*, single copy bacteriophage genes.

selected mutant phages from only the dose of chrysotile that resulted in the highest inductions over background levels. The majority of spontaneous mutants were deletions of various sizes throughout the *red BA/gam* genes (86 of 93 or 92%). Of these deletion mutants, 1 bp deletion made up 68 of 93 or 73%, whereas deletions ranging from 2 bp to 1 kb made up 8 of 93 or 8.6%. Of the spontaneous mutations with deletions 10 of 93 or 11% encompass regions of both the *gam* and *redBA* genes. In contrast, 41 of 74 or 56% and 10 of 74 or 14% of mutants recovered from chrysotile treated cells were single base pair deletion and deletions ranging from 2 bp to 1 kb, respectively. The proportion of mutants induced by chrysotile suffering loss of both the *gam* and *redBA* genes was increased from 10 of 93 or 11% among spontaneous mutants to 17 of 74 or 23% in fiber-treated MEF cells (Table 1).

Deletions > 2 kb contribute to chrysotile-induced mutagenicity. To provide further evidence of the contribution of deletions > 2 kb to the mutagenicity of chrysotile, we compared the frequencies of deletions > 2 kb induced by chrysotile at a dose of 1 μg/cm^2 with those derived spontaneously from control cultures (Table 2). Although the total Spi$^-$ mutant yield in chrysotile-treated cells was 2.4-fold higher than that of controls, the frequency of deletions > 2 kb induced by 1 μg/cm^2 of fibers was 5.2-fold higher than those derived from nontreated control (2.6 vs. 0.5×10^{-6}, $p < 0.005$). The frequency of base substitution and small deletions including single base deletions and deletions < 1 kb formed in fiber-treated MEF cells was only 2-fold higher than those from nontreated cases. These results indicated that the major types of mutations induced by chrysotile were deletions > 2 kb.

Oxyradicals mediated the mutagenicity of chrysotile in transgenic mouse mutation assay system. There is evidence that the genotoxicity/carcinogenicity of asbestos fibers is mediated by reactive oxygen/nitrogen species (Shukla et al. 2003). To demonstrate that oxyradicals mediated the mutagenicity of chrysotile fibers in MEF cells, we exposed MEF cells to either chrysotile for 24 hr in complete medium, or to H_2O_2 in serum free medium for 15 min in the presence or absence of catalase (Figure 4). The relative viability of MEF cells treated with a 1 μg/cm^2 dose of chrysotile was 71%, whereas the relative viability of MEF cells after exposing to 2.9 mM H_2O_2 was 69%. Both chrysotile and H_2O_2 led to significant increases in Spi$^-$ mutant yields in MEF cells. As shown in Figure 4, the mutation yield induced by H_2O_2 treatment was slightly higher than that of chrysotile at equal toxic doses, although the difference was not statistically significant. Furthermore, the mutation yields induced by either chrysotile at a dose of 1 μg/cm^2 or 2.9 mM H_2O_2 were dramatically suppressed in the presence of 5,000 U/mL catalase ($p < 0.05$). Interestingly, the ratio of the mutants with deletions > 2 kb was similar between chrysotile and H_2O_2 in that 20 of 84 or 24% of the mutants induced by 2.9 mM H_2O_2 lost both *redBA* and *gam* genes compared with 17 of 74 or 23% among those induced by a 1-μg/cm^2 dose of chrysotile (Figure 5). The mutant fractions with deletions > 2 kb increased from 0.5 ± 0.16 observed in controls to either 2.6 ± 0.93 or 3.2 ± 1.34 in cells treated with either chrysotile or H_2O_2, respectively. The dose of catalase used here had little effect on the level of cell viability and mutant fraction in control cells. Similarly, heat-inactivated catalase (by boiling for 10 min) had little effect on the mutant fraction in exposed cells.

Induction of γ-H2AX in MEF cells. Among various type of DNA damages, the DSBs in DNA may be the most damaging and genotoxic, which elevate the frequencies of gene translocations, rearrangements, amplifications, and deletions during repair and misrepair of DSBs (Khanna and Jackson 2001). A very early step in the response of mammalian cells to DNA DSBs is the phosphorylation of histone H2AX at serine-139 at the sites of DNA damage. To investigate whether chrysotile induces phosphorylation of H2AX in MEF cells, we exposed cultures to either a 1- or 2-μg/cm^2 dose of chrysotile for 24 hr before being fixed and stained with anti-γ-H2AX antibodies. The expression of phosphorylated H2AX as a function of DNA damage was then analyzed using flow cytometry. The histograms represented the frequency of cell number versus the intensity of the fluorescence signals of γ-H2AX antibody staining [FL1-H (green fluorescence signal received by the photomultiplier tube); Figure 6A]. Even though the number of foci/cell cannot be measured directly by flow cytometry, we found that MEF cells incubated with chrysotile showed an increased staining with anti-γ-H2AX antibodies as detected by immunofluorescence. However, there was no dose-dependent induction of γ-H2AX in MEF cells exposed to either 1 or 2 μg/cm^2 doses of chrysotile (Figure 6B). Concurrent treatment of catalase greatly suppressed the induction of γ-H2AX among treated cells. These results suggest that chrysotile induced DNA damage that triggers a stress response leading to H2AX phosphorylation.

Discussion

Asbestos fiber is an important environmental carcinogen worldwide and remains the primary occupational concern in many developing countries. Although the carcinogenicity of asbestos is well established, the underlying mechanism is not known. We have previously

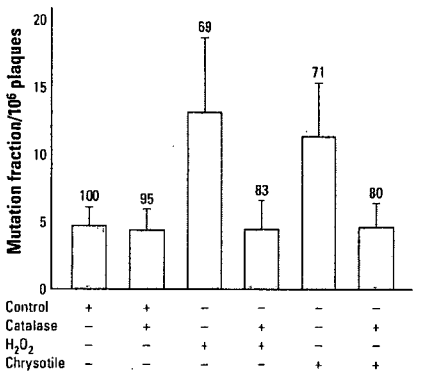

Figure 4. Mutant fractions at *redBA/gam* loci in MEF cells exposed to either chrysotile asbestos at a dose of 1 μg/cm^2 or 2.9 mM H_2O_2 either in the presence (+) or absence (–) of catalase (5,000 U/mL). Results were expressed as the total number of confirmed λ-phage mutants divided by the total number of rescued phages. The average number of preexisting mutants per 10^6 plaques used for these experiments was 4.69 ± 1.42. Numbers above error bars indicate the percentage of relative viability. Data were pooled from three to six independent experiments. Error bars indicate ± SD.

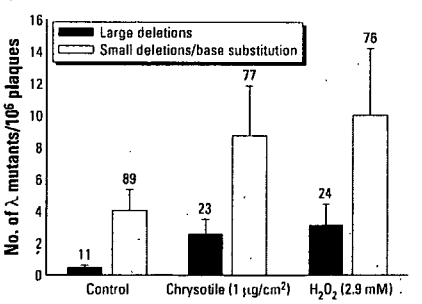

Figure 5. Mutant fractions of λ-phage mutants with specific molecular characteristics in MEF cells exposed to either chrysotile at a concentration of 1 μg/cm^2 or H_2O_2 at a dose of 2.9 mM. Numbers above error bars indicate ratio of mutation type calculated as percentage. Data were pooled from three to six independent experiments. Error bars indicate ± SD.

Table 2. Mutant fractions of deletions involving the *redBA/gam* region and other smaller deletions including single base changes in either nontreated control cells or cells treated with chrysotile fibers (1 μg/cm^2 for 24 hr).

	Control	Asbestos
Total mutant fraction at *redBA/gam* loci	4.69×10^{-6}	11.4×10^{-6}
Large deletions (> 2 kb)		
Mutant fraction	0.5×10^{-6}	2.6×10^{-6}
Increase above the control	1.0	5.2
Small deletions plus single base changes		
Mutant fraction	4.2×10^{-6}	8.8×10^{-6}
Increase above the control	1.0	2.1

demonstrated that asbestos fibers are mutagenic and induce gene/chromosomal mutations in mammalian cells. Similar results have subsequently been reported by others using various *in vitro* and *in vivo* assays that can quantify multilocus deletions (Hei et al. 1992; Lezon-Geyda et al. 1996; Park and Aust 1998). However, it has not been established how asbestos fibers induce such mutational events *in vivo*.

Inhalation studies in Big Blue *lacI* transgenic mice have revealed that there is a 1.96-fold increase in mutation frequencies in lung tissues of crocidolite-exposed mice compared with nonexposed control mice, but no specific mutant spectrum has been identified (Rihn et al. 2000). More recently, mutation induction factors ranging from 1.1 to 3.2 in the omenta have been reported in Big Blue *lacI* transgenic rats injected with crocidolite (Unfried et al. 2002). Intratracheal instillation with amosite results in a 2-fold increase in the mutation frequency in lung DNA in Big Blue *lacI* transgenic rats (Topinka et al. 2004). It should be noted that the *lacI* transgenic system is limited to small sequence alterations between 1 and 20 bp, such as point mutations, small deletions, and insertions. Most genome mutations such as large deletions and insertions, translocations, and aneuploidy cannot be effectively recovered by the *lacI* shuttle vector. Several studies in which mutation frequencies in the *lacI* transgenic system were compared with that in endogenous genes have shown that spontaneous mutation frequencies at reporter genes were dramatically higher than those found at the endogenous *hprt* gene (Skopek et al. 1995; Walker et al. 1999). It is likely that overall mutagenesis induced by asbestos fibers may be underestimated in Big Blue *lacI* mice. As such, it is extremely desirable to establish an efficient system to recover large deletion events induced by asbestos fibers *in vivo*.

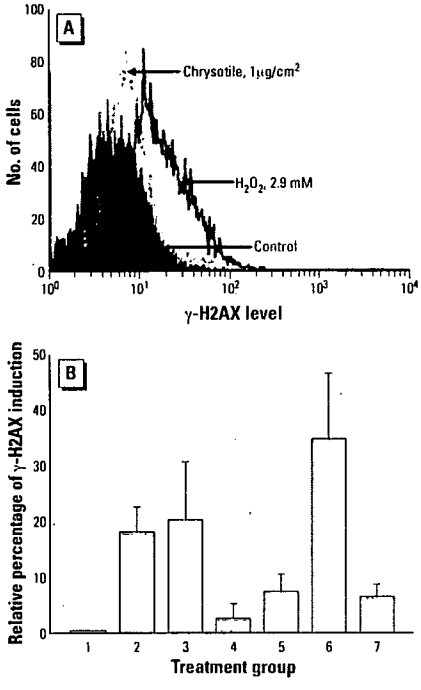

Figure 6. Accumulation of γ-H2AX in MEF cells exposed to either chrysotile for 24 hr in completed medium or H_2O_2 for 15 min in serum-free medium in the presence or absence of catalase. (*A*) Generation of γ-H2AX in cells treated with either chrysotile or H_2O_2 detected by flow cytometry using mouse monoclonal anti–γ-H2AX labeled with FITC. Results are shown using FL1-H. (*B*) Induced γ-H2AX in MEF cells exposed to either chrysotile or H_2O_2 in the presence or absence of catalase. (1) Control; (2) 1 μg/cm² chrysotile; (3) 2 μg/cm² chrysotile; (4) 5,000 U/mL catalase; (5) 1 μg/cm² chrysotile + 5,000 U/mL catalase; (6) 29 mM hydrogen peroxide; (7) 29 mM hydrogen peroxide + 5,000 U/mL catalase. Data were pooled from three independent experiments. Error bars indicate ± SD.

The *gpt* delta transgenic mouse system, established in the laboratory of one of the coauthors provides a unique opportunity to assess the *in vivo* mutagenic potential of mineral fibers (Masumura et al. 2003; Nohmi and Masumura 2004, 2005). The *gpt* delta mice carry tandem repeats of λ EG10 DNA in two units of 40 phage copies each on both arms of chromosome 17, which are retrievable as phage particles by an *in vitro* packaging reaction. The rescued phages are then used to quantify the mutation yield upon exposure to genotoxic agents. In the present study the MEF cells from the transgenic mice were used to both quantify and characterize the deletions induced by graded doses of chrysotile fibers. Our results demonstrated that chrysotiles induced a dose dependent increase in mutant yield at the *gam* and *redBA* loci in MEF cells and that the incidence and types of mutants generated were comparable to those induced by equitoxic doses of H_2O_2.

Among the mutants with deletions ≥ 2 kb that span the *redBA/gam* gene, the mutant fraction induced by treatment with a 1 μg/cm² dose of chrysotiles was 5.2-fold higher than those derived spontaneously. The mutant fraction and the number of mutants with deletions > 2 kb, however, were not elevated by further increase in fiber doses. Although the precise reason for this lack of dose–response relationship is not clear, it is possible that mutated cells were selectively killed or that the λ phages were not effectively recovered *in vitro* at high fiber doses. In addition to large deletions, the small mutational events observed were predominantly single base pair deletions at the *gam* locus in both spontaneous mutants and mutants induced by asbestos (Table 1). There is evidence that deletions in the *gam* gene not only inactivate the *gam* gene but also interfere with the translation of the *redBA* gene, leading to functionally inactivate *gam* and *redBA* genes (Masumura et al. 2003). It should be noted that the maximum size of deletions detectable by the Spi⁻ assay is 9.6 kb. However, deletions extending into regions adjacent to the transgene concatemer are not detected, as two intact cos sites are required for the packaging of a single λ vector. Our present study indicated that the maximum deletion generated by chrysotiles in the *gpt* delta transgenic mutation system were kilobase-sized intrachromosomal deletions, which were much smaller than our previous reports on megabase–sized multilocus deletions generated by asbestos in the human–hamster cells (Hei et al. 1992), largely because of the nature of the model system.

Various *in vitro* and *in vivo* studies have indicated that oxyradicals are one of the key determinants of asbestos-induced mutagenesis and carcinogenesis (Shukla et al. 2003). Among the most biologically active oxyradicals (e.g., superoxide anions ($O_2^{\bullet}$), hydroxyl radical ($^{\bullet}OH$), singlet oxygen ($^1O_2$), and hydroperoxy radical ($HO_2^{\bullet}$), H_2O_2 is relatively long-lived and directly crosses cell membranes by simple diffusion (Root et al. 1975). There is evidence that H_2O_2 not only induces damage to DNA, causing single- and double-strand breaks, base loss, base substitution, and cross-linking, but also causes chromosome and chromatid aberrations (Mondello et al. 2002). Recently, 8-hydroxydeoxyguanosine, an oxidative DNA damage marker, has been detected in Big Blue *lacI* transgenic rats treated with asbestos (Unfried et al. 2002). In an effort to understand the molecular mechanisms involved in the intra-chromosomal deletions induced by chrysotile in the present model, we compared mutation patterns between chrysotile asbestos and ROS. In the absence of serum, H_2O_2 produced predominantly $^{\bullet}OH$ radicals in human fibroblast culture (Weitzman and Graceffa 1984). Our results showed that for chrysotile-induced λ mutants the ratios of mutants with large deletions were similar to those induced by H_2O_2 at equitoxic doses. From a mechanistic point of view, these data suggest that similar mutagenic mechanisms are involved between asbestos fibers and chemically generated ROS. Consistent with this possibility, large mutational events mediated by oxyradicals have been observed in the human–hamster, AS52, and L5178 systems (Fach et al. 2003; Lipinski et al. 2000; Xu et al. 2002).

DSBs are usually regarded as the most deleterious type of DNA damage, induced either by environmental stress, such as irradiation or oxidative stress by the stalling of DNA replication forks (O'Driscoll and Jeggo 2006). Inefficient or inaccurate repair can elevate the frequencies of deletion, amplification, and chromosomal translocation, leading to chromosomal instability and neoplastic transformation. There is evidence that survival